Atmospheric Research 270 (2022) 106086

Contents lists available at ScienceDirect

Atmospheric Research

journal homepage: www.elsevier.com/locate/atmosres

# Intraseasonal scale ensemble forecasts of precipitation and evapotranspiration for the Madeira River basin using different physical parameterizations

Weslley de Brito Gomes [a,*], Prakki Satyamurty [a], Francis Wagner Silva Correia [b], Sin Chan Chou [c], Leonardo Alves Vergasta [a], André de Arruda Lyra [c]

[a] Postgraduate Program in Climate and Environment (CLIAMB, INPA/UEA), Av. André Araújo, 2936, Campus II, Aleixo, 69060-001 Manaus, Amazonas, Brazil
[b] Amazonas State University, Superior School of Technology, Av. Darcy Vargas, 1200, Parque 10 de Novembro, 69065-020 Manaus, Amazonas, Brazil
[c] National Institute for Space Research, Center for Weather Forecasting and Climate Research, Av. dos Astronautas, 1758, 12227-010 São José dos Campos, São Paulo, Brazil

ARTICLE INFO

*Keywords:*
Madeira River basin
Ensemble intra-seasonal prediction
Downscaling
Eta regional model
Bias correction

ABSTRACT

Eta Regional Model of CPTEC-INPE is used to obtain intraseasonal (30-day) 8-member ensemble forecasts over the Madeira River basin for the period 2002–2012. The initial and boundary conditions are taken from Atmospheric General Circulation Global Model in six members and from Global Coupled Ocean-Atmosphere Model in two members. The intraseasonal forecasts produced by dynamic downscaling with Eta Regional model ensemble have satisfactory skill. The skill of the ensemble mean is better than the individual members up to 15-days lead time forecasts. The ensemble mean reproduces the seasonal cycle and spatial distribution of the hydrological variables. Members with the relaxation technique of Betts-Miller-Janjic produced better results. The forecasts by the members that used Kain-Fritsch scheme presented larger deviations from observations. Substantial improvements in skill are obtained through bias correction. This is the first work to attempt dynamic downscaling over the Madeira Basin in the intraseasonal time scale for a period of 10 years. The ensemble downscaled products have potential to be fed into surface hydrological models for forecasting droughts and floods and related hydrological variables over the basin.

## 1. Introduction

The Amazon hydrological basin with an area of nearly seven million km$^2$ has the most diverse hydrological and ecological regions on the planet. The Amazon tropical forest occupies 5.3 million km$^2$, which corresponds to 40% of the total tropical forest area of the globe, and is home for 10–15% of the biodiversity of the Earth. The basin stores 150 to 200 billion tons of carbon, thereby it plays a fundamental role in the equilibrium of global climate (Fan and Miguez-Macho, 2010; Aragao et al., 2014; Latrubesse et al., 2017; Weng et al., 2018; Moran-Zuloaga et al., 2018). Due to intense evapotranspiration in the region (3–4 mm day$^{-1}$) the basin presents high rates of precipitation recycling of 25–50% which means a significant portion of the precipitation over the region is from local and regional cascade recycling (Zemp et al., 2017; Zanin and Satyamurty, 2021).

Condensation and rain formation occur in the middle troposphere while evaporation occurs at the surface. That is, solar radiation is used for evapotranspiration at the surface and latent energy is released in the middle levels. The convective activity transports energy upward in the form of latent heat. High rates of precipitation recycling means large

*Abbreviations:* AGCM, Atmospheric General Circulation Model; BH, Bolivian High; BSS, Brier Skill Score; CPTEC, Center for Weather and Climate Prediction; EQM, Empirical Quantile Mapping; RCM-Eta, Eta Regional Climate Model; ETS, Equitable Threat Score; ET, Evapotranspiration; GCM, Global Climate Model; GCOAM, Global Coupled Ocean-Atmosphere Model; HSS, Heidke Skill Score; ITCZ, Intertropical Convergence Zone; LS, Linear Scaling; SALLJ, South America Low-level Jet; MAE, Mean Absolute Error; INPE, National Institute for Space Research; r, Pearson Correlation Coefficient; PQM, Gama Quantile Mapping - Parametric; POD, Probability of Detection; PODF, Probability of False Alarm; QM, Quantile-quantile Mapping; ROC, Relative Operating Characteristic Diagram; RMSE, Root Mean Square Error; SAMS, South American Monsoon System; SACZ, South Atlantic Convergence Zone; SD, Standard Deviation; ECMWF, European Centre for Medium-range Weather Forecasts.

* Corresponding author.
*E-mail address:* wbg.mcl16@uea.edu.br (W.B. Gomes).

https://doi.org/10.1016/j.atmosres.2022.106086
Received 27 July 2021; Received in revised form 11 February 2022; Accepted 11 February 2022
Available online 17 February 2022

fluxes of latent heat. The energy cycle over the whole Amazon tropical forest controls the regional circulation and affects global general circulation, and therefore regional and global climates. If the evaporation and the transport of latent energy are altered, changes in the regional and global climates are expected (Marengo et al., 2009; Nobre et al., 2009; Zemp et al., 2017).

In the northern portion of the Amazon basin the recycling efficiency of continental evaporation is higher than in the southern portion (Van der Ent et al., 2010). The Amazon basin is a composite of several smaller basins, of which the Negro River and Madeira River basins, in that order, are more important. These two sub-basins contribute to more than 1/3 of the total runoff of the Amazon Basin into the Atlantic Ocean (Barthem et al., 2004).

Many studies show that the dry season (wet season) in the southwestern portion of the Amazon Basin is becoming longer (shorter) since the 1980s (Marengo et al., 2011; Gloor et al., 2013; Arias et al., 2015). In addition, the results obtained by Guimberteau et al. (2013) using the land surface model ORCHIDEE under the B1, A1B and A2 emission scenarios to provide flow projections in the main sub-basins of the Amazon River suggest that the Madeira River basin may experience climate extremes, i.e., extreme drought events may intensify towards the end of the 21st century. In the Madeira and in the southwestern portion of the Amazon basin widespread flooding occurred in 1992, 1993, 1997, 2007, 2008 and recently there were high precipitation and runoff in the austral summer of 2014 (Espinoza et al., 2014; Ovando et al., 2016) and in 2021.

Due to the consequences of the extreme events caused by climatic variability in the Amazon Basin, forecasting of meteorological events in the intra-seasonal time scale becomes important (Silva et al., 2006; Silva et al., 2007). Such forecasts are expected to provide valuable information for planning strategies and prevention and mitigation of disasters related to droughts and floods that may affect the environment and the economy of the region. The intra-seasonal hydroclimatic forecasts are also utilized for water management, energy generation, navigation, agriculture and cattle breeding activities (Tucci et al., 2003; Collischonn et al., 2005; Collischonn et al., 2007; Meller, 2012).

Deterministic forecasts do not inform margins of possible errors. Moreover, large variability of the hydroclimatic conditions and their uncertainties in the region require the use of ensemble prediction technique, widely used in the climate and weather prediction centers (Fan et al., 2014; Meller et al., 2014). This technique provides an interval of possible evolution of future weather conditions, thus adding to the forecasts its uncertainty and reliability metrics. This technique has become the preferred paradigm because it demonstrates improvements over the deterministic prediction with any single numerical integration (Fan et al., 2014; Schwanenberg et al., 2015; Siddique and Mejia, 2017).

In Brazil the Center for Weather and Climate Prediction (CPTEC) of the National Institute for Space Research (INPE) has been utilizing Eta Regional Climate Model (RCM-Eta for brevity) operationally for intra-seasonal numerical forecasts (Chou et al., 2005, 2012; Bustamante et al., 2006, 2012). Although the usefulness of the intra-seasonal ensemble forecasts is appreciated, an evaluation of systematic errors in the forecasts inherent to the model is an important activity in order to attribute a degree of confidence in climatic simulations (Cloke and Pappenberger, 2009; White et al., 2017). Also, it is important to find the biases in the forecasts, and to make corrections before presenting the forecasts and their uncertainties to the decision makers (Boucher et al., 2012). There are several techniques for removing or reducing this type of errors in the literature. In the intra-seasonal scale forecasts, methods employing Linear Scaling and Quantile-quantile Mapping (QM) techniques are more common for the hydrometeorological variables (Piani et al., 2010; Themeßl et al., 2012; Yuan et al., 2015; Crochemore et al., 2016).

Past studies suggest that the ability of prediction strongly depends on the region and season of interest (Liu et al., 2017; Tian et al., 2017). As such, the evaluation of the performance of intra-seasonal forecasts of precipitation and evapotranspiration for the Madeira River basin, utilizing an ensemble of forecasts with different physical parameterizations in the RCM-Eta, is considered to contribute for the understanding of the physical and hydrological processes that govern the climate and its variability. This understanding is needed for the improvement of predictive capacity of hydrometeorological variables in the Madeira River basin. In this context, the objective of the present study is to evaluate the performance and the uncertainties in the meteorological forecasts for the Madeira Basin, especially in the reproduction of extreme hydroclimatic events using different parameterization schemes. The degrees of uncertainties in the intra-seasonal forecasts produced by the atmospheric model are estimated which will help to verify improvements in the skill of the model.

## 2. Methodology

The principal characteristics of the area of interest, the Madeira Basin (Fig. 1), the model characteristics, the numerical experimental strategy adapted in this study, and the statistical techniques of evaluation of the intra-seasonal scale forecasts are presented here. The proposed ensemble prediction system is composed of (i) prediction of meteorological variables by ensemble forecasts with RCM-Eta obtained by dynamic downscaling of Global Climate Model (GCM) outputs, (ii) three methods of bias correction, and (iii) statistical verification of skill for precipitation and evapotranspiration (hereafter designated ET) forecasts.

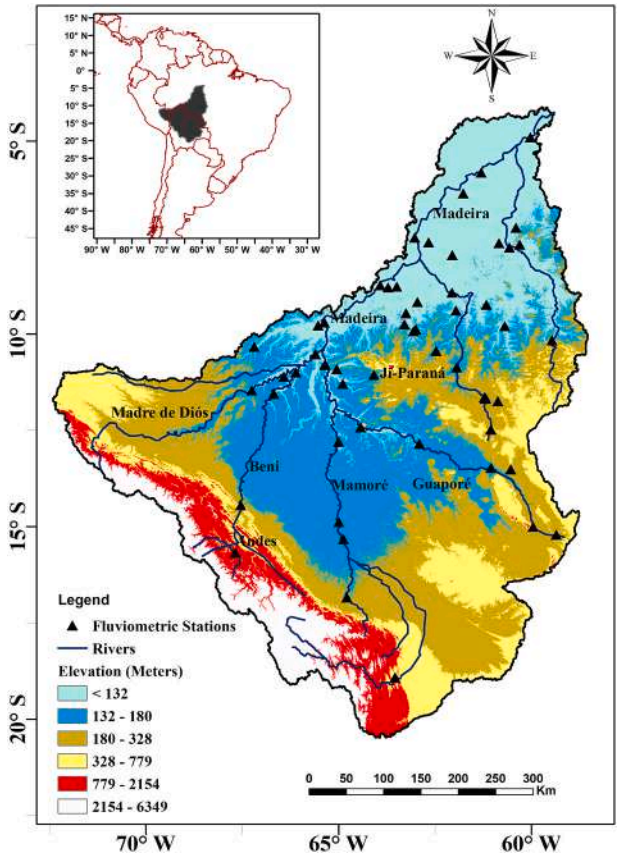


**Fig. 1.** Location and topography of the Madeira River basin. Principal rivers and tributaries are shown in blue. Hydrographic stations are marked (black triangles). [Agencia Nacional das Aguas (ANA)]. (For interpretation of the references to colour in this figure legend, the reader is referred to the web version of this article.)

### 2.1. Characteristics of Madeira River basin

The Madeira River, situated in the southwestern portion of the Amazon Basin, starts in the Andes and flows northeastward to join the Amazon River. Its basin has diverse geography, vegetation and climate. A major part, 51%, of this basin is in Bolivia, 42% in Brazil and 7% in Peru with a total area of more than $1.32 \times 10^6$ km$^2$ (Molina-Carpio et al., 2017). Its mean annual rainfall is 1940 mm and its discharge is 31,200 m$^3$ s$^{-1}$ (Molinier et al., 1995). It is composed of three climatic regions according to Koppen-Geiger classification, Af (tropical humid), Am (tropical rainy with monsoon) and Aw (warm tropical with dry season) (Beck et al., 2018). The rainfall regimes of these regions are determined by a combination of local-scale and large-scale physiographical and atmospheric circulation characteristics. It has a rainy season in austral summer (DJFM) related to the South American Monsoon System (SAMS) composed of South Atlantic Convergence Zone (SACZ), South America Low-level Jet (SALLJ) east of the Andes, Chaco Low and the Bolivian High (BH) (Marengo et al., 2004; Wanzeler da Costa and Satyamurty, 2016). The SACZ and the LLJ determine the transport of moisture from southern Amazon region to the southeastern and southern regions of Brazil. In the mean, an estimated 50% of the annual precipitation in the basin occurs in the 4-month season DJFM, January being the rainiest month (Navarro and Maldonado, 2002). The precipitation in the dry season (JJAS) is caused by cold frontal incursions from the south (Navarro and Maldonado, 2002; Amorim Neto et al., 2015). In austral summer, intense convective activity over the southwestern Amazon and the high Bolivian plateau cause the anticyclonic circulation in the upper troposphere known as Bolivian High (BH). During austral winter the Intertropical Convergence Zone (ITCZ) migrates northward, the BH disappears and the precipitation is low.

According to Molina-Carpio et al. (2017), the Madeira basin has topographical heterogeneities, ranging from 6400 m asl in its southwestern portion to 50 m asl in the eastern portion. A low lying plain area of 150 thousand km$^2$ between the tributaries Beni, Mamore and Guapore, in the upper Madeira basin, known as Llanos de Mojos, with an inclination of as little as 10 cm in one km, is inundated most of the year and is one of the largest floodplain (Guyot et al., 1996; Hamilton et al., 2002; Ovando et al., 2016; Parrens et al., 2019).

### 2.2. Eta regional climate model

The RCM-Eta developed at the Center for Weather and Climate Studies (CPTEC) of the National Institute for Space Research (INPE) (Chou et al., 2005, 2012, 2020) is utilized for obtaining the intraseasonal predictions of atmospheric variables. This model is considered adequate for limited area forecasts and satisfactorily represents mesoscale phenomena. In regions where the topography is steep this model (Mesinger, 1984) with its vertical coordinate η in stepwise formation is appropriate (Mesinger et al., 2012).

The integration scheme in the model is split-explicit. Gravity wave adjustment is made through modified forward-backward scheme by Janjic (1979) and advection term is treated by Euler-backward scheme. Spatial differentiation is treated as proposed by Janjić (1984) which controls the false flow of energy to shortwaves. The model has a complex representation of physical processes through parameterization schemes. The turbulent exchanges in the vertical are solved by Mellor and Yamada (1982) scheme with a 2.5 closure, where the turbulent kinetic energy is a predicted variable. The energy exchanges at the surface are based on the similarity of Monin and Obukhov (1954) and utilizes the Paulson (1970) stability function.

The RCM-Eta contains a set of parametrizations of different subgrid scale physical processes. The treatment of radiative fluxes in the atmosphere was developed by Geophysical Fluid Dynamics Laboratory (GFDL) in which the shortwave radiation scheme is by Lacis and Hansen (1974) and the longwave radiation scheme is based on Fels and Schwarzkopf (1975). The initial distributions of Ozone, Carbon dioxide and albedo are obtained from climatology. The surface hydrology is treated by NOAH scheme (Chen et al., 1997).

The model has four soil layers, 7 types of soil and 12 types of vegetation. The vegetation map of the model includes changes due to accelerated human activity observed in the Amazonian biome in the late 20th century (Sestini et al., 2002).

### 2.3. Ensemble intraseasonal forecast strategy

The ensemble forecast scheme used here considers variations in the forecasts due to the uncertainties in the initial conditions and also in the physical process parameterizations. The use of ensemble forecasts provides an interval of the possible evolution of atmospheric states forecast by the model, adding information about its reliability. The RCM-Eta version seasonal utilizes the convective parameterization scheme of Betts-Miller-Janjic (Janjić, 1994) – BMJ, and Kain-Fritsh (Kain, 2004) – KF, and cloud microphysics parameterization of Zhao et al. (1997) – ZHAO and Ferrier et al. (2002) – FERR. The initial and boundary conditions are provided by the Atmospheric General Circulation Model (AGCM - Cavalcanti et al., 2002) and by Global Coupled Ocean-Atmosphere Model (GCOAM - Pilotto et al., 2012), both of CPTEC-INPE (see Table 1). The resolution of the global models is T062L28, corresponding to 200 km horizontal spacing and 28 atmospheric levels in the vertical. Each integration is performed for 30 days and the anomaly of sea surface temperature persists throughout the integration, except when the GCOAM is used for the boundary conditions. In this case, the forecast SSTs are used.

For the present study, the RCM-Eta is configured with a horizontal resolution of 40 km and with 38 levels in the vertical. Its horizontal domain is limited to 15°N-50°S and 25°W-90°W and the time step used in the integrations is 90 s. The scheme of obtaining higher resolution forecasts by integrating a limited area model with the initial and boundary conditions given by a GCM is dynamic downscaling. Each numerical integration proceeds for 30 days starting from 12 UTC of the designated day of every month in the period of 10 years from 2002 to 2012. Eight numerical integrations, each with a different set of initial conditions or precipitation physics or microphysics and/or SST specified, form an ensemble as shown in Table 1. Six member integrations are run with initial and boundary conditions from AGCM. The other two members are run with conditions given by GCOAM. The first seven experiments utilize BMJ convection scheme. The eighth member utilizes KF scheme. All but the first and the last members use Zhao microphysics and the other two use Ferrier parameterization. The starting dates of integration of the members vary from 13th to 17th of the month. Uncertainty in initial conditions is related to errors in observations and deficiency in data assimilation methods. Although the errors may be small, they can lead to large errors in weather and climate forecasts due to the chaotic nature of the atmosphere. Making several forecasts with slightly different initial values provides a sense of how different the forecast may be if the initial condition exhibits an error (Lorenz, 1963).

To evaluate the representation of the RCM-Eta in terms of precipitation and evapotranspiration in the Madeira Basin the MERGE data (Rozante et al., 2010) and the Global Land Evaporation Amsterdam Model - GLEAM data (Miralles et al., 2011; Martens et al., 2017) are used.

The MERGE consists of the interpolation of observed precipitation data from approximately 4000 rain gauges spatially distributed over South America along with satellite precipitation estimates. The technique has as its main objective reduction of uncertainty and bias in precipitation data, especially for regions with a low density of observed data, such as the Amazon basin (Rozante et al., 2020). Daily precipitation data (accumulated over 24 h) with a spatial resolution of 20 km are used for this study (available at: http://ftp.cptec.inpe.br/modelos/tempo/MERGE/GPM/DAILY/).

GLEAM (www.gleam.eu) consists of a set of algorithms that uses land cover and other satellite measurements to estimate the different

**Table 1**
Characteristics of members in the ensemble with different physics parameterizations, global model and initial conditions.

| Member | Convection scheme | Microphysics parameterization | Designation of member experiment | Inicial/boundary conditions | Date CI |
|---|---|---|---|---|---|
| Member1 | Betts-Miller-Janjic | Ferrier | BMJFA15 | AGCM | 15 |
| Member2 | Betts-Miller-Janjic | Zhao | BMJZA13 | AGCM | 13 |
| Member3 | Betts-Miller-Janjic | Zhao | BMJZA14 | AGCM | 14 |
| Member4 | Betts-Miller-Janjic | Zhao | BMJZA15 | AGCM | 15 |
| Member5 | Betts-Miller-Janjic | Zhao | BMJZA16 | AGCM | 16 |
| Member6 | Betts-Miller-Janjic | Zhao | BMJZA17 | AGCM | 17 |
| Member7 | Betts-Miller-Janjic | Zhao | BMJZO15 | GCOAM | 15 |
| Member8 | Kain-Fritsch | Ferrier | KFFO15 | GCOAM | 15 |

components of evapotranspiration (Miralles et al., 2011; Martens et al., 2017). Here we use GLEAM version v3.5a, which covers the period from 1980 to 2020 at a spatial resolution of 0.25° × 0.25° and daily temporal. For the analysis, we use actual evapotranspiration (ET, mm day$^{-1}$), which is defined as the sum of transpiration, bare soil evaporation, open water evaporation, interception loss, and snow sublimation.

### 2.4. Bias correction

In order to eliminate or decrease substantially systematic biases from raw RCM-Eta outputs and produce useful information for hydrometeorological variables (precipitation and evapotranspiration) in the Madeira Basin, three different methods of Bias Correction (BC), namely, Linear Scaling (LS) by Lenderink et al. (2007), Empirical Quantile Mapping (EQM) by Themeßl et al. (2012), and Gamma Quantile Mapping - Parametric (PQM) by Piani et al. (2010), are used to correct the biases of RCMs on a daily timescale. For the sake of better comparability among methods, all of them were calibrated on daily basis using a moving 30 day window centered on each day, producing a transference function for each day of the year. For instance, a window of 30 days results in 300 values for a 10-year period of calibration. The observed precipitation threshold for the determination of a wet day was $\geq$1 mm day$^{-1}$. These methods are briefly described below. The skill assessment and bias adjustment of model data were performed using the open-source R package climate4R (Iturbide et al., 2019, see also www.meteo.unican.es/climate4R), a R-based framework for postprocessing (which includes the package downscaleR for statistical downscaling; Bedia et al., 2020).

#### 2.4.1. Empirical quantile mapping (EQM)

The 'quantile mapping' tries to adjust the distribution of the data simulated by the RCM-Eta in such a way that those data have the same quantile distribution as the observational data. To achieve this, a transference function (TF) is applied, which maps the simulated data to have the same statistical moments as the respective observed cumulative distribution.

$$P_{prev}^{BC}(t) = CDF_{obs,d}^{-1}\left(CDF_{prev,d}\left(P_{prev}(t)\right)\right) \quad (1)$$

where $P_{prev}{}^{BC}(t)$ and $P_{prev}(t)$ are bias corrected data and simulated data from the RCM-Eta during the reference period (also known as the calibration period), and $CDF_{prev,\ d}$ and $CDF_{obs,\ d}{}^{-1}$ are predicted and observed cumulative distribution functions for each day $d$, respectively.

EQM makes non-linear corrections of the mean, variance, quantiles and frequencies, preserving the intensities of the extremes in such a way that the adjusted data has the same pattern as the climatological data. A limit on daily precipitation can be imposed to avoid distortions in the frequency distribution due to trace precipitation such as drizzle. For the case of precipitation, the minimum observed precipitation amount for a day to be considered wet was 1.0 mm day$^{-1}$. The EQM is based on the supposition that the observed datasets and the model simulated datasets follow the same kind of distribution which may possibly introduce new biases. If non-parametric empirical CDFs are introduced without any other supposition about the precipitation distribution, the method is known as Empirical Quantile Mapping (EQM).

#### 2.4.2. Gamma quantile mapping - parametric (PQM)

The quantile mapping can also be used to adjust the RCM-Eta ensemble predictions substituting the empirical CDFs by a parametric distribution. Similar to EQM, we can assume that both the RCM-Eta simulated precipitation data and the observed precipitation data follow a specific distribution, a commonly used distribution for precipitation is Gamma which is a function of two parameters: α and β, which define the form and scale of the distribution, respectively, as shown in Eq. (2).

$$f\gamma(x|\alpha,\beta) = x^{\alpha-1}\cdot\frac{1}{\beta^{\alpha}\cdot\Gamma(\alpha)}\cdot e^{\frac{-x}{\beta}}; x \geq 0; \alpha,\beta \succ 0 \quad (2)$$

where Γ(α) is the Gamma function and α controls the distribution profile and β determines the dispersion of the Gamma distribution and $x$ represents RCM-Eta values of daily precipitation.

#### 2.4.3. Linear scaling (LS)

The linear scaling method is based on the calculation of a multiplication correction factor between the climatological normals obtained from observational datasets and the simulated normals for the period of study. The simulated data is modified by imposing the mean monthly values to match perfectly the long term observed means. The precipitation data is generally adjusted through a multiplication factor, keeping the same mean as the observational data. The linear scaling operates monthly correction values based on the differences between the observed control data and the unadjusted data:

$$P_{cor,d} = P_{prev,d} \times \frac{\mu\left(P_{obs,d}\right)}{\mu\left(P_{prev,d}\right)} \quad (3)$$

where $P_{cor,d}$ and $P_{prev,d}$ are corrected and uncorrected precipitation data, respectively, and μ represents Mean (parameter of Gaussian distribution) of the expected value for the moving interval of 30 days around the day 'd'.

Although several studies (Shrestha et al., 2015; Teng et al., 2015; Shrestha et al., 2017) utilized the linear scaling technique, it tends to overvalue the extreme events in the same way as does with more common events, because the whole series is multiplied by the same factor, the monthly correction coefficient, which may affect statistical characteristics of the adjusted data.

### 2.5. Evaluation metrics of ensemble predictions

For this study, we selected deterministic and probabilistic verification metrics in order to facilitate the verification of the ensemble forecasts. Deterministic verification metrics evaluate the ensemble mean forecast, while probabilistic metrics help to evaluate the forecast probabilities, including the ensemble spread (Brown et al., 2010). Intra-seasonal Forecast quality is assessed using a wide range of attributes, including bias, Error and accuracy (Mean Absolute Error – MAE; Root

Mean Square Error - RMSE), spatial correlation (Pearson Correlation Coefficient - r), Skill (Brier Skill Score – BSS; Equitable Threat Score – ETS; Heidke Skill Score - HSS), discrimination (Relative Operating Characteristic Diagram - ROC), according to Brown et al. (2010), Demargne et al. (2010) and Wilks (2011). Details of both deterministic and probabilistic skill scores are given in Appendix A.

## 3. Results and discussion

### 3.1. Ensemble precipitation forecast verification

For the evaluation of the precipitation forecasts over the Madeira River basin, the statistical metrics are calculated for each individual member prediction as well as for the ensemble mean. The observational data means are obtained from MERGE. The mean values of the statistics are obtained for the spatial average of the basin and for the whole period of study and the results are shown in Fig. 2.

The bias, MAE and RMSE of member KFFO15 and for the first few days of forecast member BMJZO15 (see Table 1) are very high compared to members BMJZA13–17, BMJFA15 and the ensemble average. The members with the BMJ parameterization and the Zhao cloud microphysics produced less bias, MAE and RMSE compared to the rest of the members.

The KFF015 overestimated the quantity of precipitation by about 36% in relation to the observed values, being the only scheme producing more rainfall than the value observed in the area of the present study (Fig. 2a). The other members produced about 15% less rainfall. Fig. 2b shows that the correlation diminishes with the range of forecast. Fig. 2b shows that smaller correlation also could be associated with higher values of RMSE.

In general, the ensemble average performs better, except for the BMJZA members with initial conditions of day 15, 16 and 17 which perform better for the first 10 days of forecasts as seen in the metrics, relative to the performance of the other individual members (Fig. 2c). The simulations with BMJ relaxation method present more realistic values of precipitation as seen in smaller values of bias than those produced by KF.

For the evaluation of the ability of the prediction scheme to discriminate the rain and no-rain events for individual member integrations (i.e., deterministic forecasts), the set of hits is plotted against the set of false alarms for producing ROC (Fig. 3). For a system of efficient forecasts, in which the number of hits are far greater than false alarms, the curve inclines towards the upper left corner. If the curve is near the diagonal, the system does not produce useful information. And, if the curve is below the diagonal, the system is useless.

For determining the capacity of intraseasonal forecasts to discriminate events of low ($> 1{,}0$ mm day$^{-1}$), moderate ($> 5.0$ mm day$^{-1}$), high ($> 10.0$ mm day$^{-1}$) and intense precipitation ($> 15$ mm day$^{-1}$), Fig. 3 presents ROCs for the individual members and for the ensemble mean.

For the low and moderate categories of precipitation the discrimination is better than in the cases of high and intense precipitations. (By discrimination we mean the model's ability of recognizing the categories of rain events). RCM-Eta presents difficulties in forecasting extreme precipitation events as also found in Tanessong et al. (2012). However, the ensemble mean and the members with BMJ and ZHAO and AGCM could discriminate better than those members with GCOAM at all ranges of forecast.

The ETS and HSS metrics for precipitation forecasts up to 30 days for thresholds ranging in 1.0 mm from 1.0 to 20 mm are shown in Fig. 4a and b, respectively. These metrics represent the skill of the model to predict precipitation at different lead times. The longer the lead time the lower the skill expected. Except for members using Ferrier scheme and those with conditions given by GCOAM, all others scored ETS $\geq 0.2$ and HSS $\geq 0.25$ up to 9 days lead time. The scores, in general, fall from the highest values for one-day lead up to 12-days lead time. That is, the ability of the model to predict the rainfall intensity decreases after 12-days lead time. However, there are upward jumps around 18-days lead and after 27-days lead. The scores of the ensemble mean increase from lead times of one day to four days and fall thereafter, and there is no jump after 27 days lead.

The scores for different ranges of precipitation threshold values from 1 to 20 mm day-1 for all forecasts (lead time of 30 days) issued are shown in Fig. 4c, d. The scores decrease rapidly for thresholds of precipitation greater than 6 mm day$^{-1}$. That is, there is good agreement between the forecasts and the MERGE data for days with rainfall not greater than 6 mm day$^{-1}$. The ensemble mean has the best scores in the interval 2 mm day$^{-1}$ to 7 mm day$^{-1}$. As is already known the scores decrease for more high precipitations (Walker et al., 2019; Chou et al.,

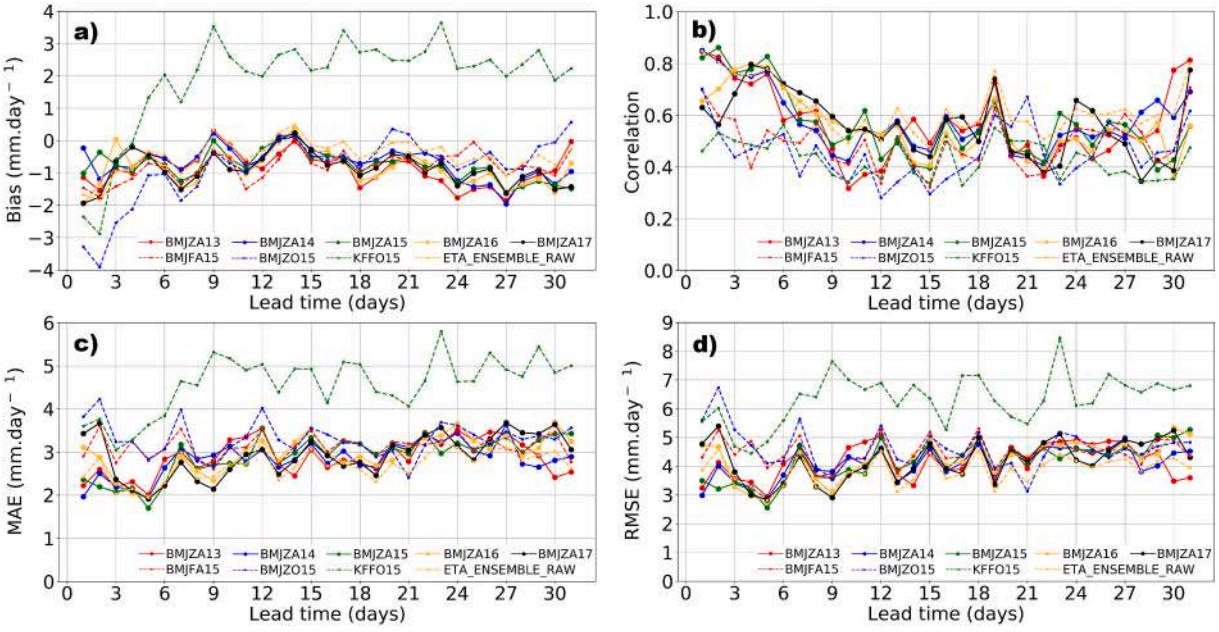


**Fig. 2.** Bias (a), Correlation Coefficient (b), MAE (c), and RMSE (d) for the 9 members and for the ensemble mean produced by RCM-Eta without bias correction. Lead time refers to the range of forecast.

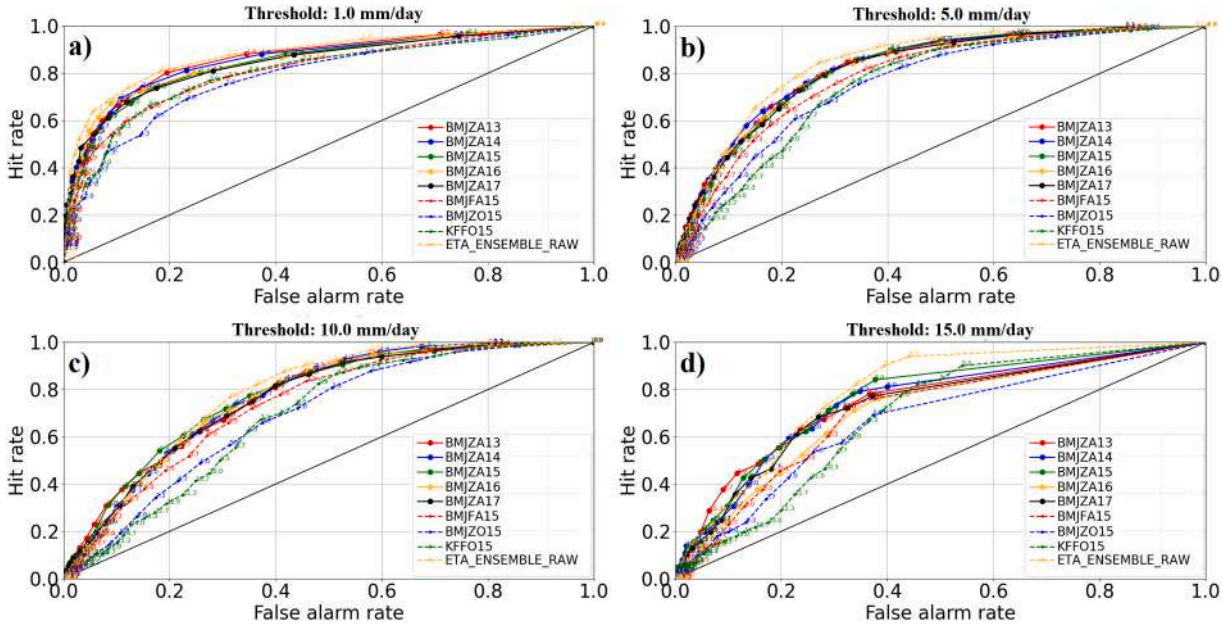


**Fig. 3.** Relative Operational Characteristics (ROC) curves for forecasts in different thresholds of precipitation. Colors indicate different members. Curve for the ensemble mean is also presented.

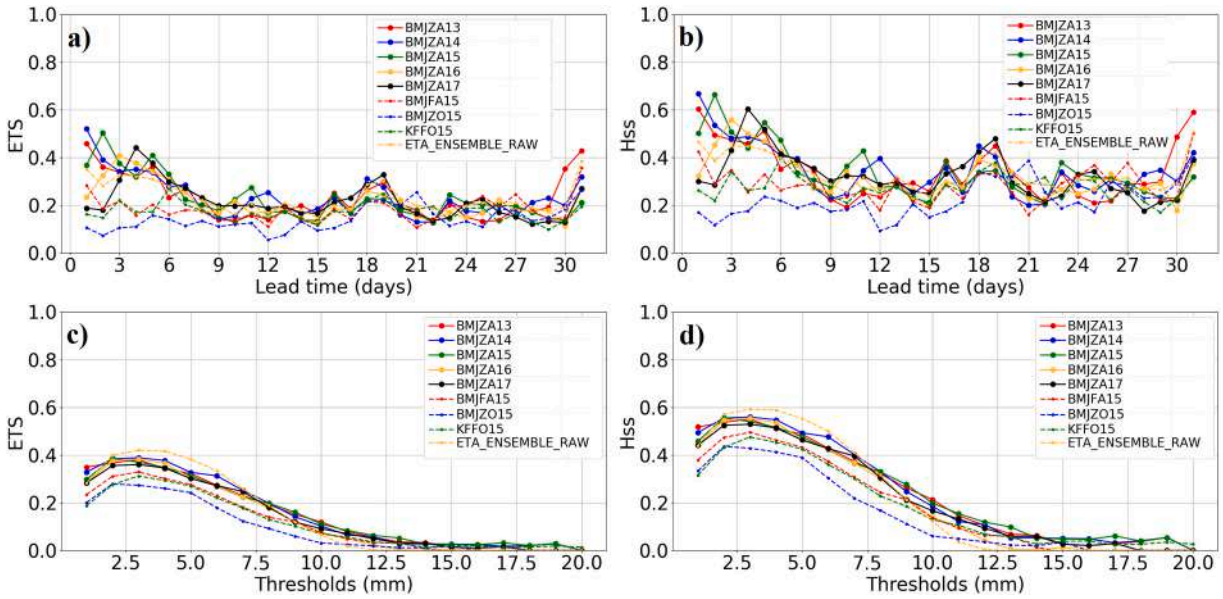


**Fig. 4.** ETS (a and c) and HSS (b and d) for the RCM-Eta downscaled forecasts without bias correction. Top row: for lead times. Bottom row: for precipitation thresholds.

2020) and for longer lead times in all numerical model outputs. However, for higher thresholds of precipitation the members with BMJ parameterization have better scores. The ensemble mean has inferior scores for higher thresholds. That is, for high rainfall events ($P \geq 10$ mm day$^{-1}$) ensemble mean is not the best choice.

The basin-mean annual cycles of rainfall for the eight members and for the ensemble mean without and with bias correction are shown in Fig. 5. For calculating the monthly means over the Madeira Basin, the whole period of 10 years of the present study, 2002–2012, is used. Fig. 5 (a) shows that the member with GCOAM using Kain-Frisch parameterization scheme overestimated the precipitation with respect to MERGE data in almost all months. Nevertheless, the ensemble mean is close to the climatological mean. All the members represented the annual cycle fairly well. Fig. 5(b), (c) and (d) show the cycle after bias corrections. The agreement with the MERGE data seasonal cycle has improved considerably. The improvement in the case of the bias correction using linear scaling is better.

The benefits of considering the ensemble mean forecasts are apparent because the mean error of the ensemble is less than the individual deterministic member forecasts. With the technique of correcting the bias the estimates of a few members simulating excessively wet conditions are improved and are adjusted close to the observed monthly means. In general, all the three techniques of bias correction improved the forecasts. However, although simple in its concept, the linear scaling worked better than the other two, because we are making corrections to the mean values.

The Taylor diagrams of the RCM-Eta forecasts which summarize the model performance, separately for the wet (DJF) and dry (JJA) periods,

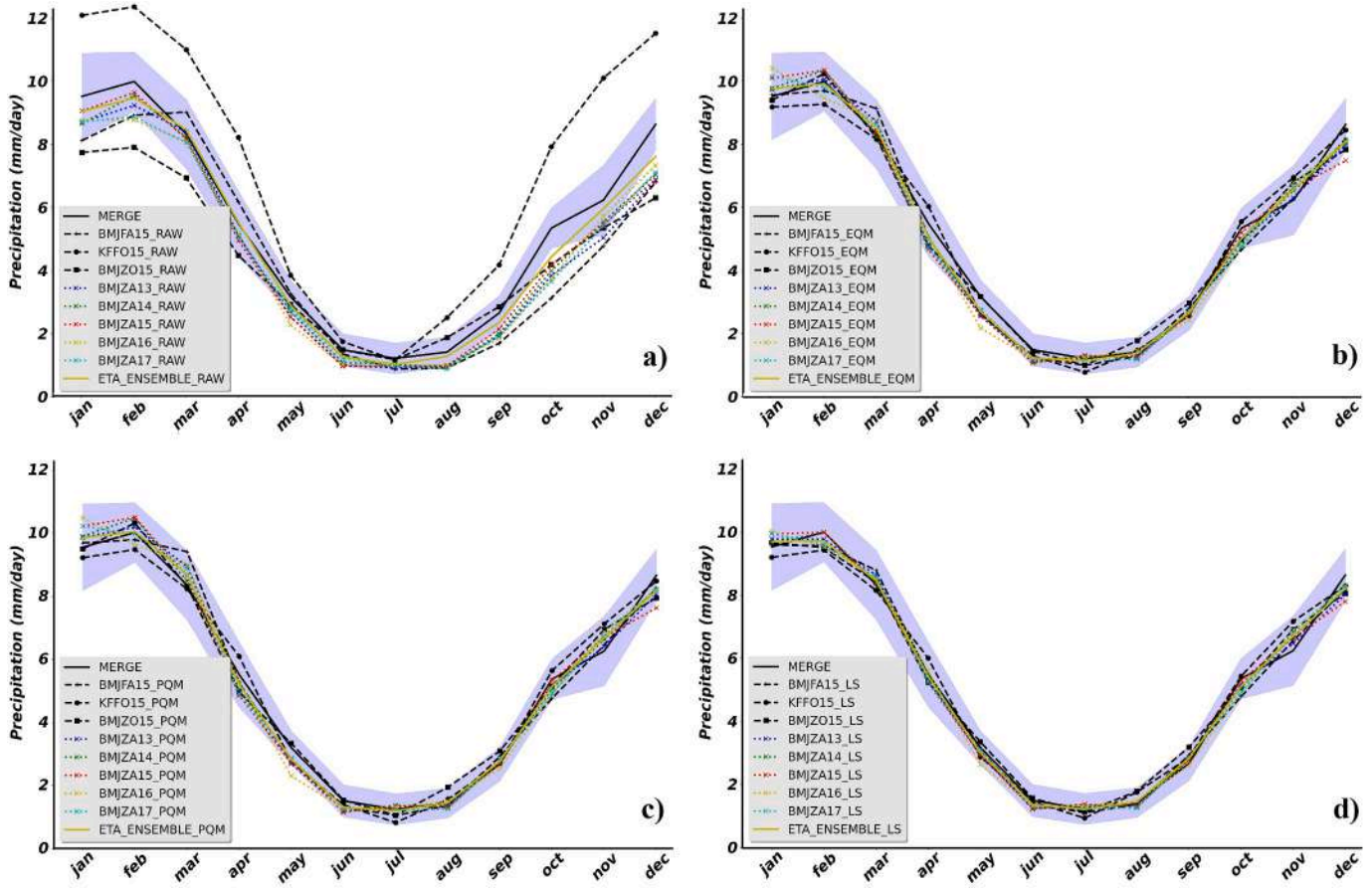


**Fig. 5.** Seasonal cycles of 10-year mean precipitation obtained from MERGE, the ensemble mean and the individual members: (a) before bias correction, (b) after EQM, (c) after PQM, (d) after LS. The blue shading represents the standard deviation. (For interpretation of the references to colour in this figure legend, the reader is referred to the web version of this article.)

are given in Fig. 6. The figure shows that in the large majority of forecasts the bias corrections improved considerably the performance of the model in both wet and dry seasons, in terms of the correlation coefficient and standard deviation. The standard deviations after the corrections are closer to the observed standard deviations. All the three methods of bias correction show the same improvements. However, the LS correction performs better.

Fig. 7 shows the spatial distributions of precipitation obtained from MERGE and the biases of the ensemble forecasts without applying the systematic error correction, ENSEMBLE_ETA_RAW, and after applying

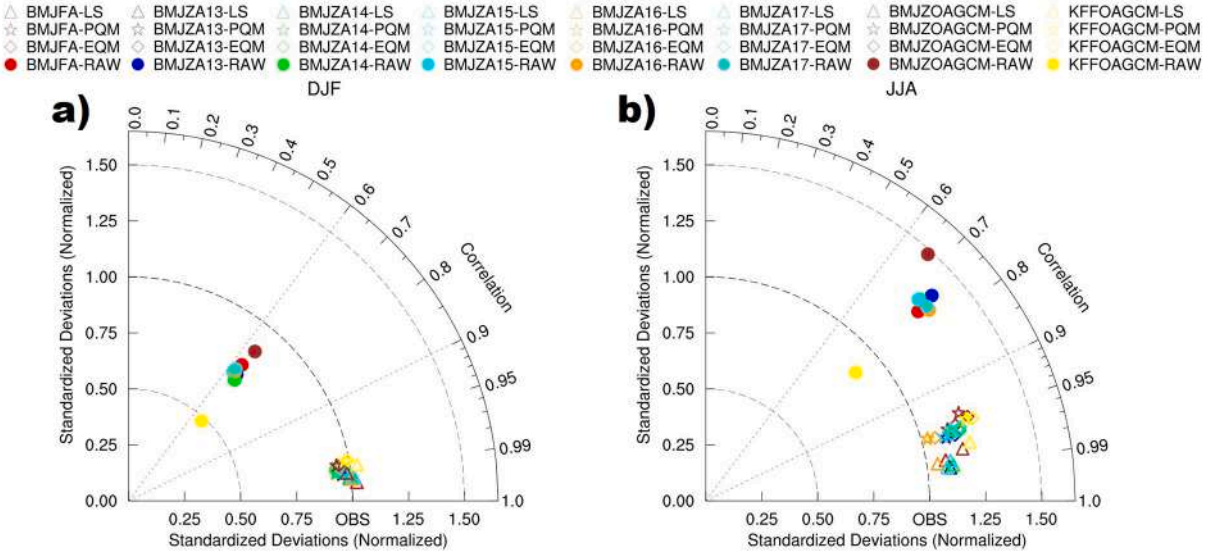


**Fig. 6.** Taylor Diagram representing spatial correlation and standard deviation for wet, DJF (left) and dry, JJA (right) periods, for individual members and for the ensemble mean with and without bias corrections.

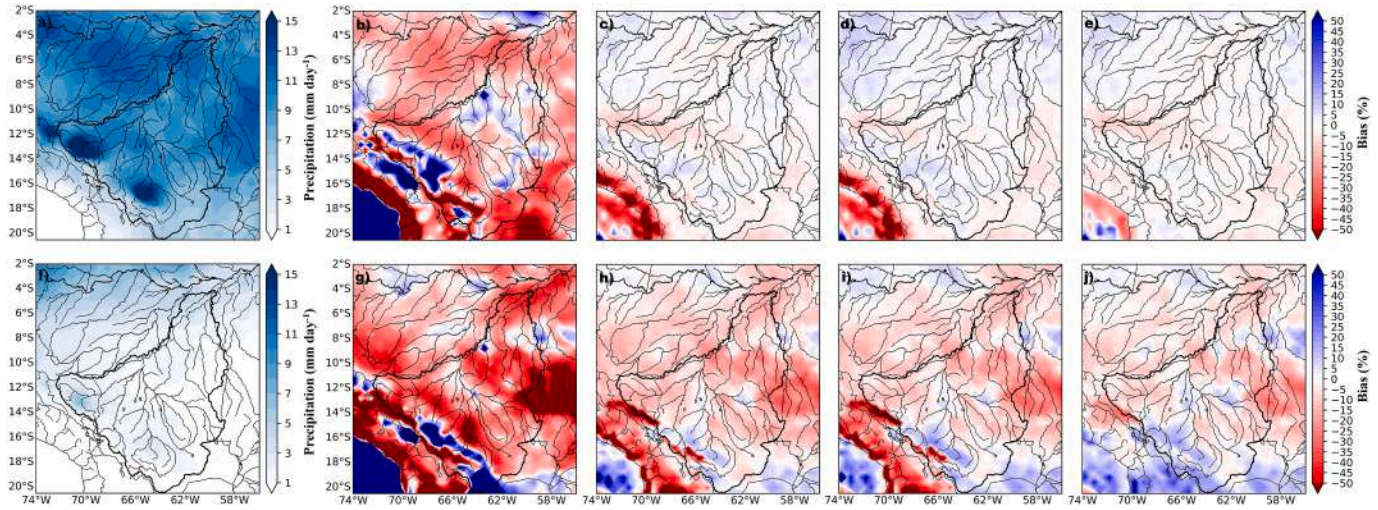


**Fig. 7.** Spatial distribution of mean precipitation (mm day$^{-1}$) (2002−2012) for the wet (a) and dry (f) seasons obtained from MERGE. Bias (%) in the ensemble mean obtained by RCM-Eta, without correction (raw) for wet (b) and dry (g) seasons. Bias after correction: (c) wet and (h) dry for EQM; (d) wet and (i) dry for PQM; (e) wet and (j) dry for LS.

the corrections, ENSEMBLE_ETA_EQM, ENSEMBLE_ETA_PQM, and ENSEMBLE_ETA_LS, for the dry and wet seasons. The RCM-Eta represented the spatial variation of precipitation over the Madeira Basin in both the seasons. Over the Madeira Basin higher precipitations occur in DJF due to the southerly position of the ITCZ and the formation of SACZ. The forecasts by RCM-Eta without bias correction underestimated precipitation compared to observations over most of the basin, except in the central and southern portions of the basin where the forecasts overestimated (Fig. 7b). In the dry season (JJA) higher precipitation values occur in the central and southern portions of the basin. In contrast to the wet season predictions, the model underestimated precipitation over nearly the entire basin and overestimated it in a narrow area of the Andean slope (Fig. 7g).

Higher positive biases are seen over the upper portions of the basin over the Andes Mountains in both the seasons, showing that the RCM-Eta presents difficulty in representing precipitation in steep slope areas. The observational datasets are considered reliable and are consistent with the topography of the region. However, there are fewer observational data points in the high mountains. The figure shows implicitly that there is a relation between the topography and the model bias.

All the three techniques of bias correction effectively improve the forecasts obtained by the RCM-Eta. However, there are differences in the three techniques in terms of reduction of bias. The spatial distribution of biases found after the corrections by EQM and PQM are similar, agreeing with Li et al. (2010). The performance of the LS method for bias correction on a monthly or seasonal scale rather than daily, although simple in its concept, is as good as or better than the techniques that use quantile adjustments. However, it is important to remember that the quantile mapping adjusts the mean, the variance, the intensity and wet and dry day frequencies of the forecasts in addition to the mean.

Another important improvement by the bias correction methods is the adjustments of the topography-dependent biases in the RCM-Eta forecasts. Here, we note that the topography related biases are almost removed, as was observed by Piani et al. (2010). At great altitudes (upper portion of the basin) the forecasts without correction show large overestimations of precipitation. On the other hand, in the low lying flat areas (*Llanos de Mojos*), the forecasts of the model are characterized by underestimations of mean precipitation in both wet and dry seasons. These are perhaps due to systematic errors in the convection parameterization scheme to represent small scale effects and clouds at higher elevations in the model as was observed by Chou et al. (2005). Such underestimations and overestimations are effectively corrected by bias correction techniques used here (Fig. 7).

Fig. 8 shows the mean errors and pattern correlation of the ensemble mean precipitation forecast by the RCM-Eta in the Madeira Basin, as functions of the lead time, without bias correction and after bias correction using the three methods described in the Methodology section. The Mean Absolute Error and the spatial correlation as well as

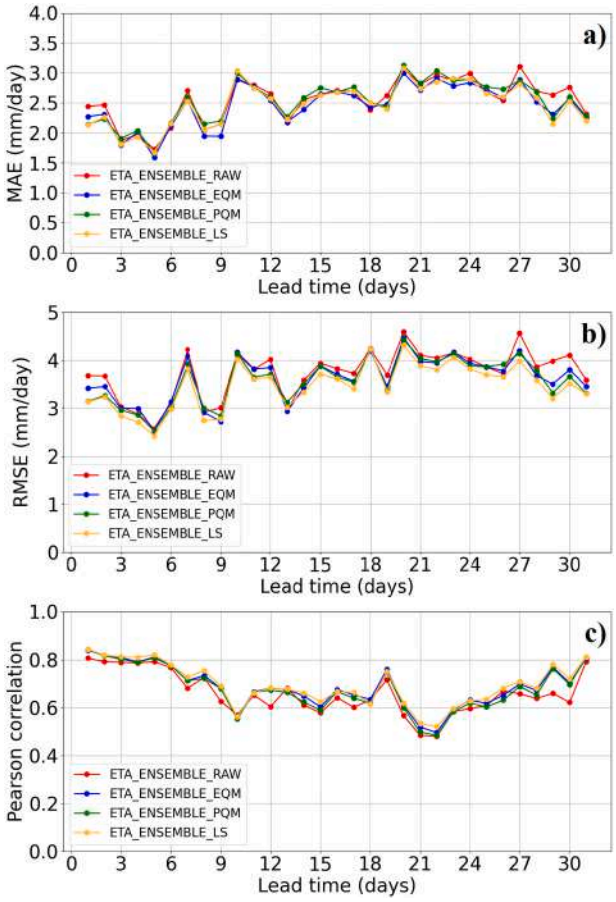


**Fig. 8.** MAE (mm day$^{-1}$) (a), RMSE (mm day$^{-1}$) (b) and Correlation Coefficient (c), of the ensemble mean forecast of RCM-Eta, without bias correction, and after bias correction by the three techniques, EQM, PQM and LS.

RMSE of the predicted precipitation reflects the quality of the forecast due to the increase of systematic error with lead time. The forecasts after bias correction using LS present the best result, with the mean correlation coefficient of 0.69, better than PQM and EQM. Zhao et al. (2017) mentioned that imposing the correlation coefficient to remain unaltered is the weakest point in EQM technique of bias correction. A comparison of the statistical metrics before and after the bias correction shown in Fig. 8, indicate that the bias corrections performed well to increase the correlation between the predicted and observed data. Also, the MAE and RMSE are reduced, although some errors remain.

In order to examine the capacity of the forecast system and discernibility between the intense rain, rain and no-rain events, ROC diagrams are presented for distinct intervals of precipitation in Fig. 9. The ROC curves for the three bias-corrected forecasts are all close to each other. The ROC curve for the forecasts in the precipitation interval 0 to 1.0 mm day$^{-1}$ without bias correction (Fig. 9a) is also close to the rest of the curves. But, the curves for forecasts without correction at higher precipitation rates move towards the diagonal. That shows that bias correction is necessary for improving the forecasts of moderate and high precipitations. There is higher reliability for less high rainfall events even without bias correction.

The Taylor diagrams and error shown in Fig. 10 present the quality of the forecasts in terms of Centered Root Mean Square Error (CRMSE), bias, correlation coefficient and standard deviation, all in one place. Bias and CRMSE arise from decomposition of RMSE, where the systematic and the unsystematic part of the RMSE are shown. In Fig. 10b, the distance of a point on the curve from the origin is equal to RMSE, all bias correction methods reduce the unsystematic error in the predictions. LS and PQM seem to reduce the precipitation systematic error closer to zero than EQM. All the three methods of bias correction improve the quality of forecasts considerably as can be seen from the reduction of mean errors and from the standard deviation (SD) of the forecasts approaching the climatological observed SD and the increase in the spatial correlations between the forecasts and the observations. The magnitude of improvements in the three methods of correction are comparable.

In order to establish the ability of the intra-seasonal forecast system, the BSS for different lead times of prediction and for different intervals of precipitation rates are calculated. The scores are presented in Fig. 11 and, in general, they decrease with lead time up to day 10 and stabilize with small ups and downs up to day 17 (Fig. 11a, c, e). The scores attain minimum values at lead time of 22 days. Later, the scores increase up to 30-days lead time. Why the scores increase rapidly at lead times longer than 22 days needs investigation. Another important aspect is that the scores are highest for events of precipitation of 3 mm day$^{-1}$ and for higher rates of precipitation the ability decreases sharply reaching very low scores for high and intense rains events. The HSS is higher than 0.3 for moderate and light precipitation events of less than 8 mm day$^{-1}$ (Fig. 11f). In all the panels the curves in yellow in comparison with other curves show that the scores (representing the ability of the forecast system) after bias correction of the forecast data using the LS method obtains higher values. The average-based bias correction method (LS) does not specifically consider daily extremes (thresholds above 15 mm day$^{-1}$) of precipitation. Intense precipitation is adjusted using the same multiplicative correction factor as light precipitation. Therefore, HSS and ETS for intense precipitation corrected by LS is lower compared to the PQM method (Fig. 11d, f). These results are in agreement with Verkade et al. (2013) who have analyzed the effect of bias corrections by different methods on the ECMWF forecast system. Also, Kolachian and Saghafian (2019) evaluated the precipitation forecasts given in S2S of ECMWF after postprocessing using the quantile mapping method. They concluded that the bias corrected forecasts show good ability of predicting monthly precipitations over most areas of Iran.

### 3.2. Ensemble evapotranspiration forecast verification

The 10-year mean spatial distribution of evapotranspiration over the Madeira Basin for the wet (DJF) and dry (JJA) seasons forecast by the RCM-Eta ensemble along with the corresponding percentage bias in relation to the GLEAM data is presented in Fig. 12. The figure also presents the percentage bias without applying the systematic error correction and after applying the corrections. In general, the RCM-Eta ensemble is able to represent the spatial distribution of ET. The forecast magnitudes vary from 3 to 5 mm day$^{-1}$. The mean of the ensemble overestimated ET over most parts of the basin in both the seasons by about 30 to 40%. As is observed in the GLEAM data, higher seasonal variation of evapotranspiration is forecast over the southern portion of the basin, influenced by the availability of solar energy.

Larger biases are seen over the slopes of the Andes and near the

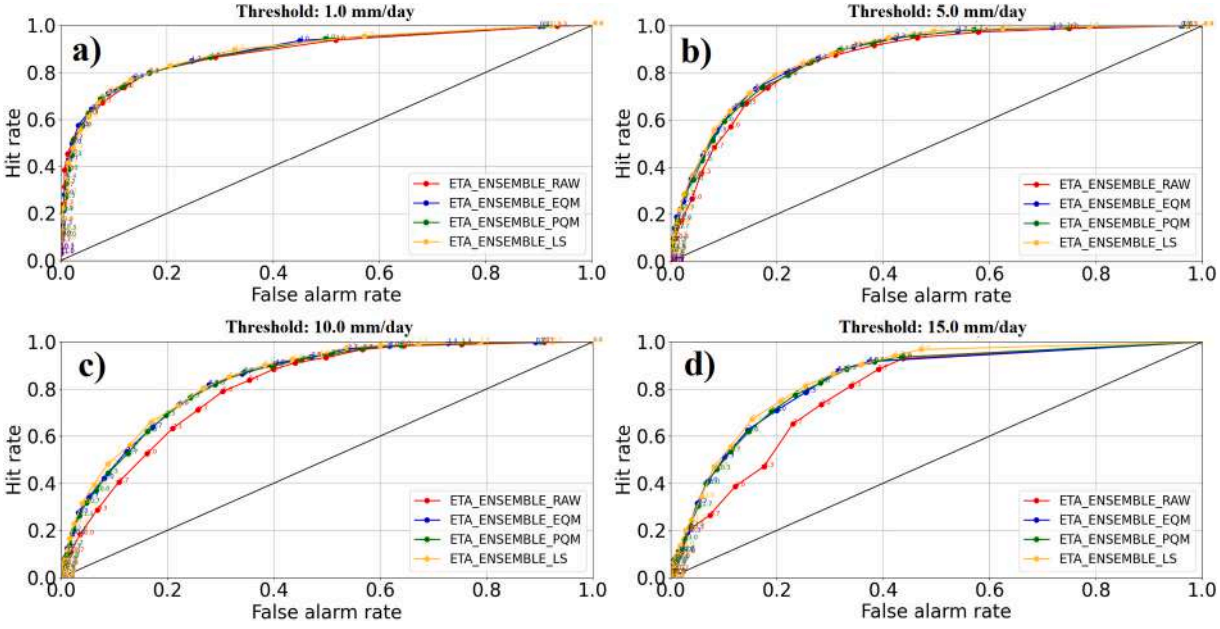


**Fig. 9.** Relative Operational Characteristics curves (ROC) for the ensemble mean forecast from RCM-Eta without bias correction and after bias correction by the three methods, EQM, PQM and LS.

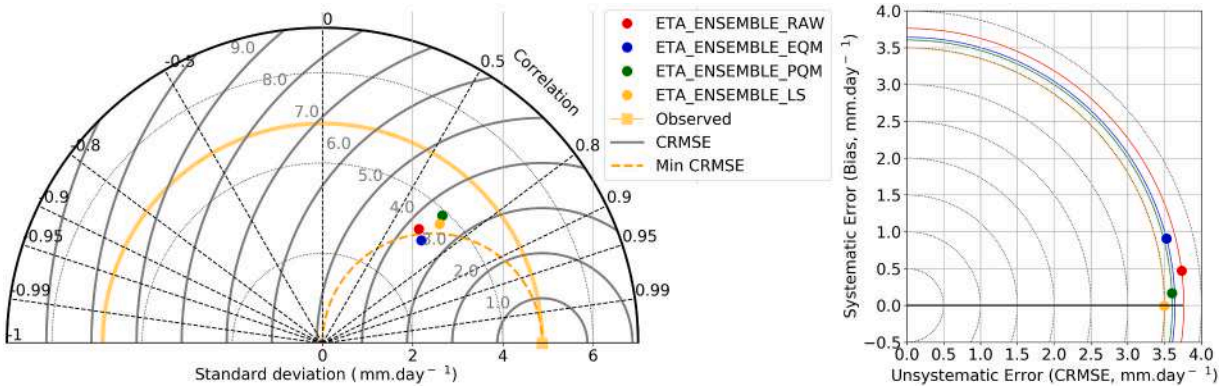


**Fig. 10.** Taylor diagram (a) Represents the spatial correlation as the azimuthal angle (dashed lines), lines of CRMSE are given in grey and forecast standard deviation by the standard deviation of the observations on the x-axis (orange circle is observed) and (b) Error diagram with contributions from systematic and unsystematic errors to the RMSE of the ensemble mean of the RCM-Eta, without and with bias corrections by EQM, PQM and LS.

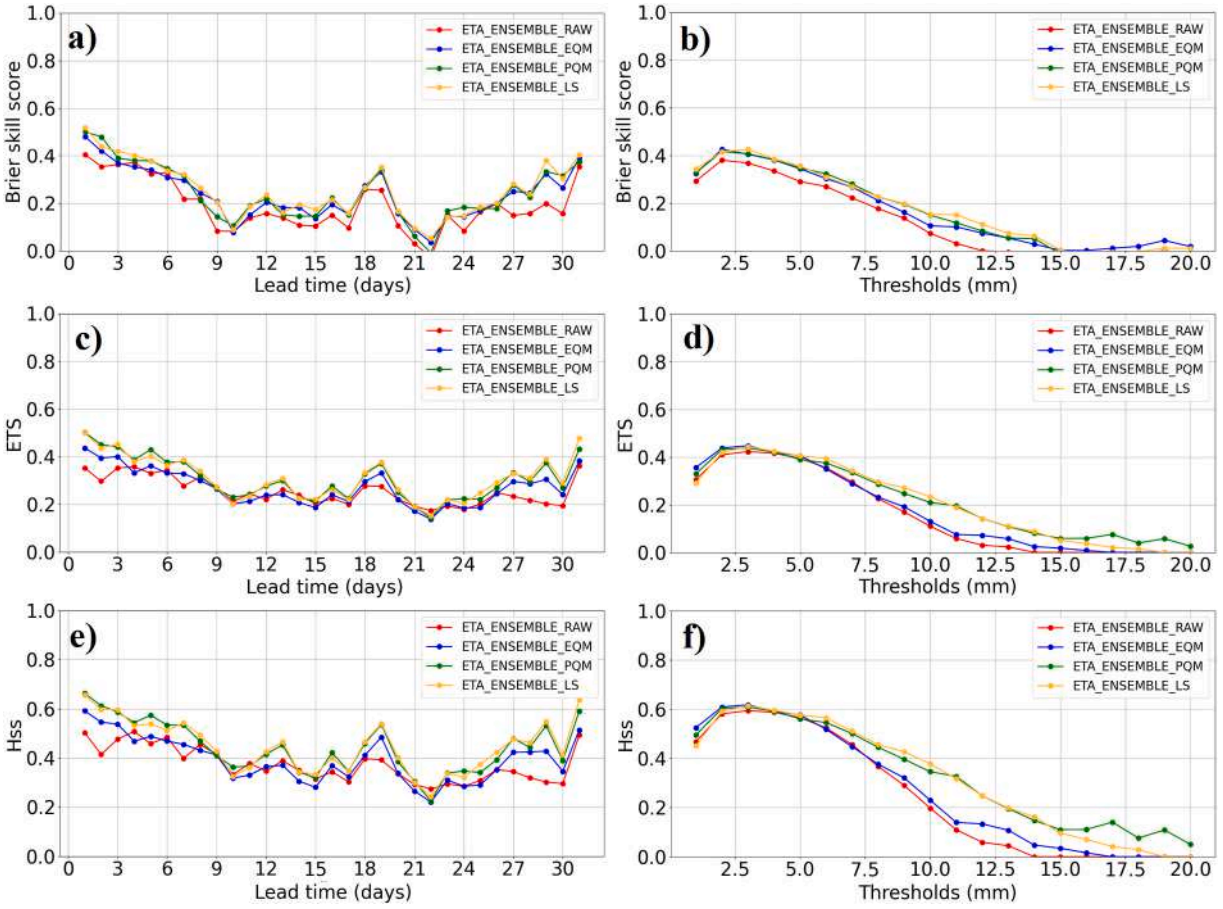


**Fig. 11.** BSS, ETS and HSS for the ensemble mean precipitation forecast by the RCM-Eta, without and with bias correction by EQM, PQM and LS. Left column: scores as functions of forecast lead time (ranging in 1.0 mm from 1.0 to 20 mm). Right column: scores as functions of rainfall for all forecasts (lead time of 30 days).

confluence of Madeira River with the main stream of the Amazon River. The bias correction, however, reduced the biases by less than 5% in the wet season and around 10% in the dry season over the Madeira Basin. The dry-season percentage biases are larger because the evapotranspiration is smaller. It is noteworthy to observe that the large biases observed in the slopes of the Andes in the southwestern portion have reduced substantially after the correction, in both the seasons.

The 10-year mean annual cycle of the individual member integrations and the ensemble mean forecasts of ET, before and after bias correction, along with the corresponding GLEAM observation values are shown in Fig. 13. All the individual members and the ensemble mean overestimated evapotranspiration in all the months of the year in relation to the GLEAM datasets (Fig. 13a). The dispersion between the members, except one member with KFF-GCOAM, is small. After the bias correction the ensemble mean as well as the individual members represented the seasonal cycle very satisfactorily.

For the evaluation of evapotranspiration forecasts over the Madeira River basin, statistical metrics are calculated for each individual member forecast as well as for the ensemble average. The observational data means are obtained from GLEAM. The mean values of the statistics are

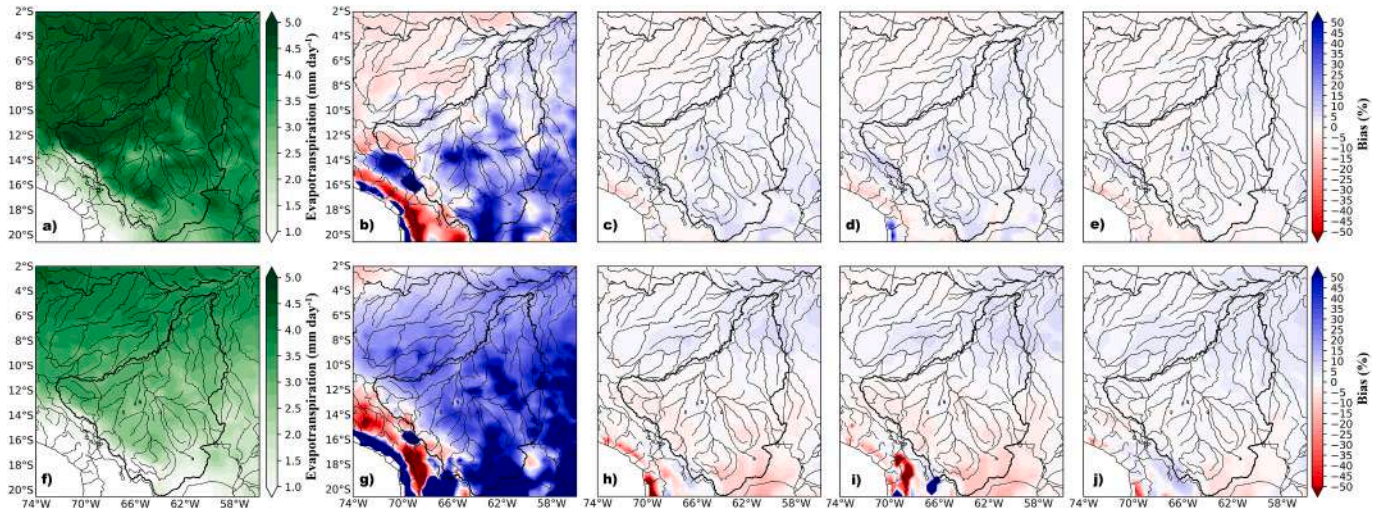


**Fig. 12.** Spatial distribution of mean evapotranspiration (mm day$^{-1}$) for 2002–2012 for (a) wet and (f) dry seasons obtained from GLEAM datasets. Bias (%) of the ensemble mean obtained by RCM-Eta without bias correction (raw), (b) wet and (g) dry seasons. Bias of the ensemble mean after correction: by Linear Scaling: for (c) wet and (h) dry for EQM; (d) wet and (i) dry for PQM; (e) wet and (j) dry for LS.

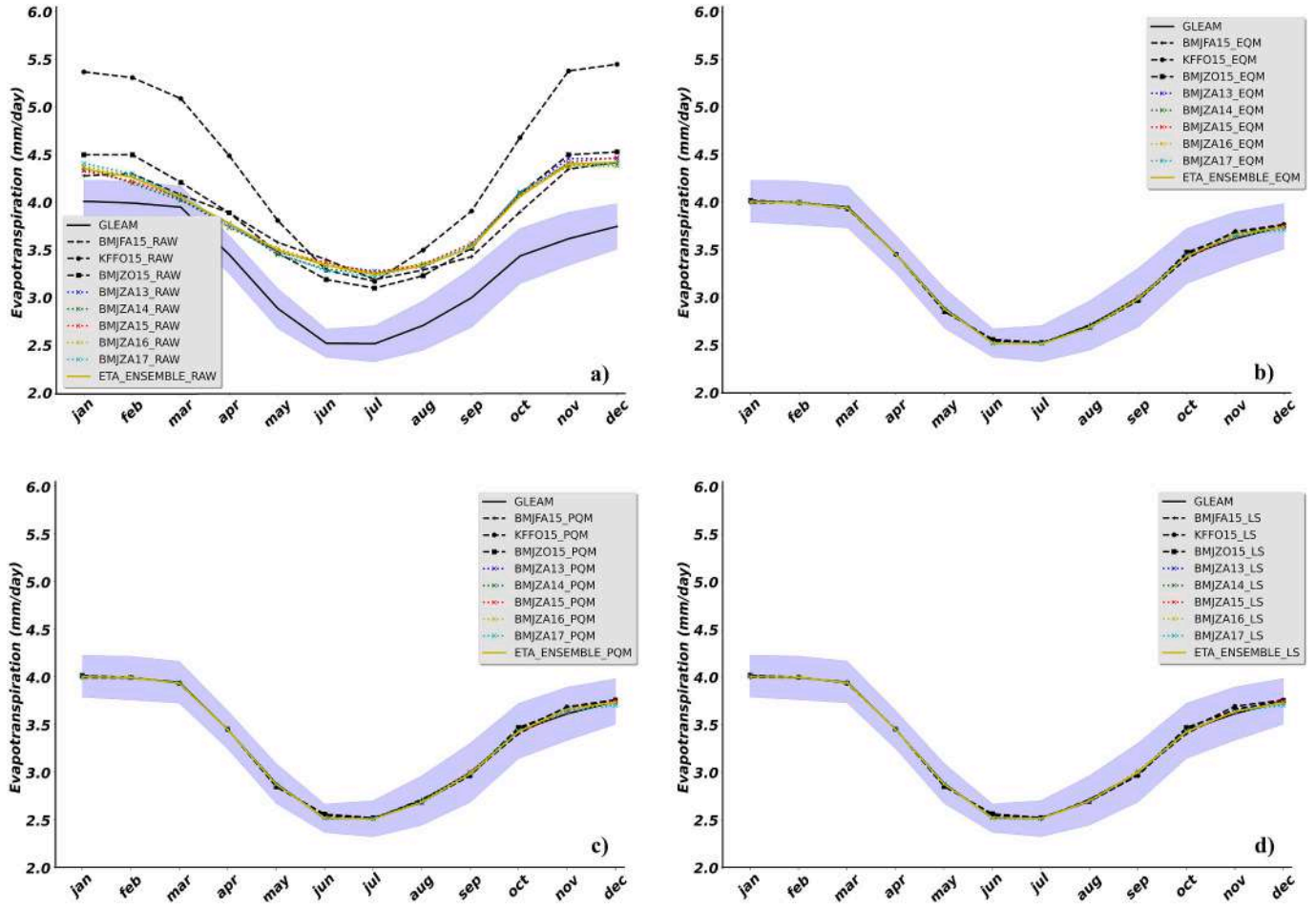


**Fig. 13.** Seasonal cycle of mean Evapotranspiration in the period 2002–2012, obtained from GLEAM datasets, the ensemble mean and the individual member integrations obtained by the RCM-Eta. (a) without bias correction, and after bias correction by (b) after EQM, (c) after PQM, (d) after LS. The blue shading represents the standard deviation. (For interpretation of the references to colour in this figure legend, the reader is referred to the web version of this article.)

obtained for the spatial average of the basin and for the entire study period and the results are shown in Fig. 14.

The bias, MAE and RMSE of the member KFFO15 and for the initial days of member BMJZO15 are very high compared to members BMJZA13–17, BMJFA15 and the ensemble average. The members with the BMJ parameterization and the Zhao cloud microphysics produced

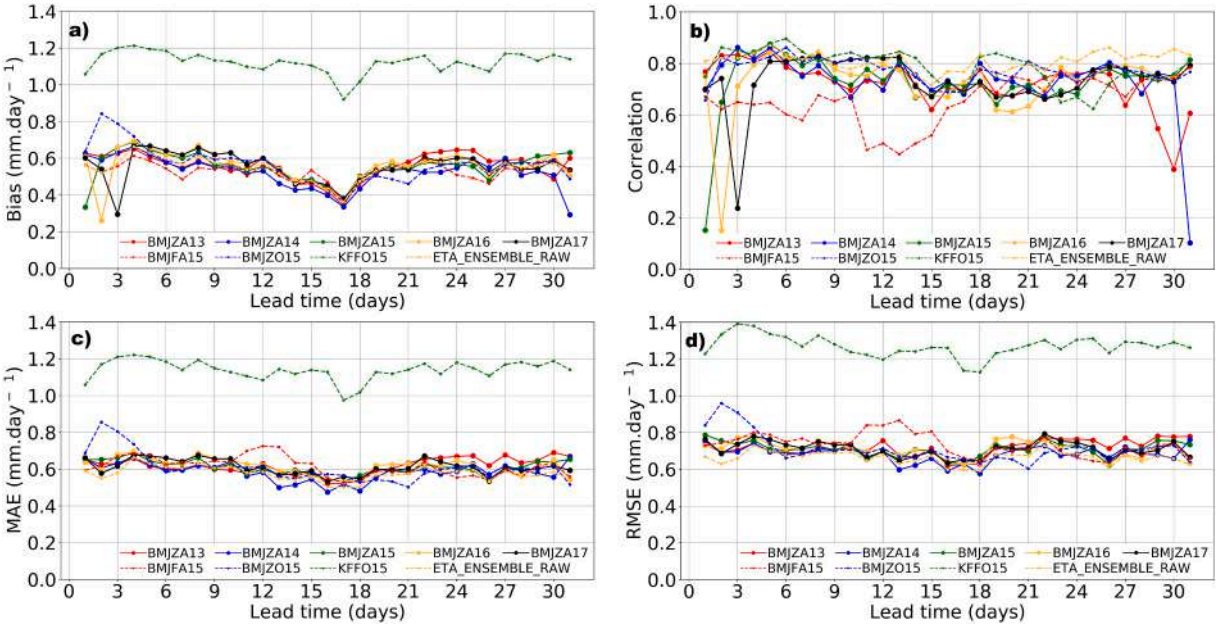


**Fig. 14.** Bias (a), Correlation Coefficient (b), MAE (c), and RMSE (d) from evapotranspiration for the 9 members and for the ensemble mean produced by RCM-Eta without bias correction. Lead time refers to the range of forecast.

less bias, MAE and RMSE compared to the rest of the members.

KFF015 overestimated the amount of evapotranspiration by about 1.0 mm day$^{-1}$ relative to the observed values, being the only scheme that produced more precipitation and consequently a higher availability of soil humidity which altered the partitioning of energy at the surface, and produced less heat for heating the air (sensible heat) than for plant transpiration and evaporation of water at the surface (latent heat) (Fig. 14a). The other members overestimated evapotranspiration by about 0.6 mm day$^{-1}$. Fig. 14b shows that the correlation decreases with the prediction interval. However, for the average of the members the spatial correlation increases starting on forecast day 21. Member BMJF15 has the lowest spatial correlation with the observed field.

In general, the ensemble average performs better, except for the BMJZA members with initial conditions of day 14 perform better between forecast days 11 and 19, as shown in the metrics relative to the performance of the other individual members. Relative to the different parameterizations, KF shows higher evapotranspiration values in the intra-seasonal forecasts (Fig. 14c). Simulations with the BMJ relaxation method show more realistic precipitation values, as seen in smaller bias values than those produced by KF.

Fig. 15 shows the MAEs, RMSE and spatial pattern correlation of the ensemble mean evapotranspiration predicted by RCM-Eta in the Madeira Basin as functions of lead time, without bias correction and after bias correction using the three methods described in the Methodology section. The predictions after bias correction using LS show the best result, with the average correlation coefficient of 0.85, better than PQM and EQM. A comparison of the statistical metrics before and after bias correction presented in Fig. 15, indicates that the bias corrections performed well to increase the correlation between the predicted and observed data. In addition, the MAE and RMSE are reduced, although some errors remain with respect to the observed GLEAM data.

## 4. Summary and conclusions

Madeira River basin is an important contributor to the total drainage of the Amazon Basin. Extreme flood and drought events in the basin affect the hydrological cycle of adjoining regions as well as the local population. High resolution precipitation and evapotranspiration forecasts on the intra-seasonal time scales are necessary for feeding the surface and atmospheric hydrological models for forecasting the river level, drainage and the area of inundation. The RCM-Eta in ensemble mode with eight members is used to downscaling the forecasts of atmospheric variables over the Madeira Basin up to 30 days, during the 10-year period 2002–2012. The initial and boundary conditions are provided by two different global models. The members of the ensemble are distinguished by the global model, the parameterization schemes for microphysics and convection and the starting date and time (see Table 1 for details). The mean performance characteristics of the precipitation and evapotranspiration forecasts over the basin obtained by the individual members as well as by the ensemble mean are thoroughly analyzed using the statistical metrics widely used in global centers of meteorological and climatological forecasts and studies.

One of the conclusions is that the intraseasonal forecasts produced by dynamic downscaling with RCM-Eta ensemble have satisfactory skill. The skill of the ensemble mean is better than the individual members up to 15-days lead time forecasts. The member which used the global ocean-atmosphere coupled model GCOAM showed less skill. With respect to different parameterizations, members with the relaxation technique of Betts-Miller-Janjic produced better results. The forecasts by the members that used Kain-Fritsch scheme presented larger deviations from observations. It is important to note that the Kain-Fritsch scheme was used in only one boundary condition and with one microphysics scheme.

Another important conclusion is that bias correction is necessary for improving the skill scores substantially and reducing the Mean Absolute Error (MAE) and Root Mean Square Error (RMSE) in the precipitation and evapotranspiration forecasts. The Relative Operational Characteristics (ROC) have shown improvement after bias correction. All the three techniques used in this study to reduce model bias improved the forecast skills and other performance metrics. The linear scaling (LS) technique for bias correction, although simple in its concept, is as good as or better than the techniques that use quantile adjustments.

The anomaly correlations between the forecasts and the corresponding MERGE observational precipitation data remained above 0.6 up to 9 days. The correlation after 18 days of forecasts showed an increasing trend and reasons are to be investigated. In general, the downscaling with regional model along with bias correction brought improvements in the forecasts of spatial distribution which shows that

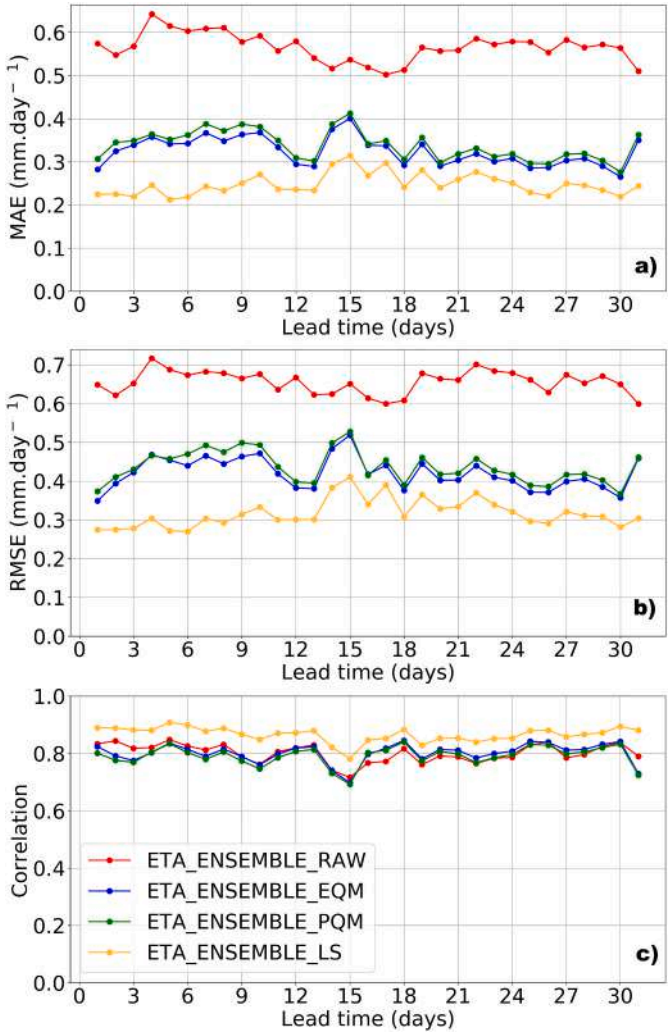


**Fig. 15.** MAE (mm day$^{-1}$) (a), RMSE (mm day$^{-1}$) (b) and Correlation Coefficient (c) from evapotranspiration, of the ensemble mean forecast of RCM-Eta, without bias correction, and after bias correction by the three techniques, EQM, PQM and LS.

the local orographic and surface characteristics influence the precipitation and evaporation. However, over steep slopes of the Andes some significant biases persisted even after corrections.

The present study is the first to attempt dynamic downscaling over the Madeira Basin in the intraseasonal time scale for a period of 10 years. The ensemble downscaled products have potential to be fed into surface hydrological models for forecasting droughts and floods and related hydrological variables over the basin.

## Declaration of Competing Interest

The authors declare that they have no known competing financial interests or personal relationships that could have appeared to influence the work reported in this paper.

## Acknowledgments

This study was financed in part by the Fundação de Amparo à Pesquisa do Estado do Amazonas (FAPEAM) - Finance Code: 01.02.016301.00268/2021. This work is developed in the Postgraduate Program in Climate and Environment (CLIAMB) jointly coordinated by the Amazon State University (UEA) and the National Institute of Amazonian Research (INPA). The first author thanks the FAPEAM for the doctoral grant. PS thanks CAPES for granting him Visiting Professorship at INPA under the PVNS program (Process n° 23038.019802/2018-07) and CNPq for the grant of PQ 306.595/2013-3. All authors thank the Center for Weather Forecasting and Climate Studies - National Institute of Space Research (CPTEC/INPE) for making available the numerical integrations datasets and the Laboratory of Terrestrial Climate System Modeling (LABCLIM/UEA) for providing the computational infrastructure - TAMBAQUI Cluster.

## Appendix A. Verification metrics

### A.1. Mean absolute error

This index gives the mean accuracy of the prediction system, given by

$$MAE = \frac{1}{N}\sum_{t=1}^{N}\left|P_{prev(t)} - P_{obs(t)}\right| \quad (A.1)$$

where N is the number of observations, $P_{obs(t)}$ is observed precipitation at the instant $t$ and $P_{prev(t)}$ is the precipitation given by the member at the same instant of time. This metric is used to measure the mean error between the deterministic prediction or ensemble prediction and the observed data.

### A.2. Root mean square error

The RMSE is used to evaluate the magnitude of the error of a deterministic forecast and is given by

$$RMSE = \left[\frac{1}{N}\sum_{t=1}^{N}\left(P_{prev(t)} - P_{obs(t)}\right)2\right]^{1/2} \quad (A.2)$$

It has the advantage of retaining the units of the variable predicted and includes the effects of the model bias and the estimated variance. It

represents the magnitude of mean difference between the forecast and the observation. RMSE near zero means the forecast is perfect.

### A.3. Correlation coefficient (r)

The Pearson correlation coefficient measures the strength of linear association between two variables. Here, we consider the relation between n pairs of predicted and the corresponding observed data and is given by

$$r = \frac{\sum_{t=1}^{N}\left(P_{prev(t)} - \overline{P}_{prev(t)}\right)\left(P_{obs(t)} - \overline{P}_{obs(t)}\right)}{\sqrt{\sum_{t=1}^{N}\left(P_{prev(t)} - \overline{P}_{prev(t)}\right)2}.\sqrt{\sum_{t=1}^{N}\left(P_{obs(t)} - \overline{P}_{obs(t)}\right)2}} \tag{A.3}$$

where N is the number of pairs of data and the overbar means the sample mean. The correlation theoretically varies from $-1$ to $+1$. $r = +1$ means the two variables are perfectly and positively related. Positive relation means, if one variable increases the other also increases. A negative relation is the opposite. r $= -1$ means that the relation is perfect except that they are negatively related. $r = 0$ means that the two variables are unrelated.

### A.4. Brier skill score (BSS)

The Brier score index measures the mean quadratic error of probability for the occurrence of a discrete event, and is given a reference interval. This index is analogous to the RMSE of a deterministic forecast except it considers the probabilities. It is given by

$$BS(L) = \frac{1}{n}\sum_{t=1}^{n}(pprev_t - pobs_t)2 \tag{A.4}$$

where $L$ is a reference interval analyzed, $pprev_t$ is the probability predicted at the instant $t$. In this case, the probability $pprev_t$ is equal to the fraction of the members that exceed the value of precipitation $L$ at the given instant, $pobs_t$ is the observed probability at instant $t$ ($pobs = 1$ if the event occurs, $pobs = 0$ if the event does not occur). The total number of forecast/event pairs n is simply the sum of these counts. BS assumes values 1 or 0, 1 for the case when the event (exceeding the value L) occurred, and 0 for the case the event did not occur. BS tells us if the predicted value agrees with the observation in exceeding a certain value of precipitation at a given instant (or on a given day).

A forecast which has excellent relation with the observations in terms of exceeding or not a given or prescribed value of precipitation, the BS equals 0. However, rare events which exceed the prescribed values may give a false impression of agreement with observations. For this reason, a modified score called Brier Skill Score (BSS) as given by

$$BSS = 1 - \frac{BS_{prev}}{BS_{ref}} \tag{A.5}$$

is preferred instead. This provides a measure of skill of the forecast system in comparison with a reference forecast which is usually the climatology.

### A.5. Relative operating characteristics (ROC) diagram

The ROC measures the capacity of the ensemble forecast system to discriminate the happening or not of events of precipitation within prescribed limits. For this purpose, a 2 × 2 contingency table is constructed for describing the distribution of simultaneous occurrences of predictions and observations (Table A.1).

**Table A.1**
Contingency table used for defining relative operating characteristics diagram (ROC) and Heidke Skill Score (HSS).

| | Observed | | |
|---|---|---|---|
| | Precipitation | No Precipitation | Marginal of Fcst |
| Forecast | a (hits) | b (false alarms) | a + b (yes fcsts) |
| | c (misses) | d (correct rejects) | c + d (no fcsts) |
| Marginal of Obs | a + c (yes obs) | b + d (no obs) | n = a + b + c + d |

a is the number of hits of precipitation events, d is the number of hits of no precipitation events, b is false alarm and c miss.

Based on the table, two indices called probability of detection (POD) and probability of false detection (POFD) are calculated:

$$POD = \frac{a}{a+c}, (= 1, \text{perfect})$$

$$POFD = \frac{b}{b+d}, (= 0, \text{perfect}) \tag{A.6}$$

The POD indicates the frequency of correct forecasts (i.e., occurrence is predicted) and POFD the frequency of false forecasts (i.e., the event predicted did not occur). In the ROC diagram pairs of POD and POFD are plotted for each interval of the variable. The diagonal line on the graph is the limit for the prediction system skill. That is if there are more correct forecasts than false forecasts, the system is considered having some skill.

### A.6. Equitable threat score (ETS)

The ETS measures the fraction of events correctly predicted (hits) after discounting the random hits and is given by

$$\text{ETS} = \frac{\text{H} - \text{CH}}{\text{F} + \text{O} - \text{H} - \text{CH}} \tag{A.7}$$

in which $CH = \frac{F^*O}{n}$.

Here CH is the expected number of hits in a random forecast. F is the number of events of precipitation predicted above a certain threshold, O is the number of events of precipitation observed above the threshold, H is the number of hits and n is the total number of events.

### A.7. Heidke skill score (HSS)

The HSS is a statistic frequently used to provide an idea of the relative quality of the forecast. The reference forecasting system is the proper climatology obtained from the historical observational series or a system based on persistence (Doswell III et al., 1990). The index measures the skill of the simulation/forecast to foresee correctly the precipitation in relation to the standard utilized, as if the forecast is made randomly. The index eliminates the influence of random hits. The index uses the proportion of correct forecasts as metric for calculating the relative quality of the forecast system, also obtained after elaborating the contingency table (Table A.1). From this table, the index is defined as

$$HSS = \frac{2^*(a^*d - b^*c)}{[(a+c)^*(c+d) + (a+b)^*(b+d)]} \quad (A.8)$$

This index varies between −1 and 1. HSS = −1 indicates that the model is incapable and HSS = 1 indicates that the model is perfectly capable. HSS = 0 means that the mean historical values are as good as the model predictions.

## References


Amorim Neto, A.D.C., Satyamurty, P., Correia, F.W., 2015. Some observed characteristics of frontal systems in the Amazon Basin. Meteorol. Appl. 22 (3), 617–635. https://doi.org/10.1002/met.1497.

Aragao, L.E., Poulter, B., Barlow, J.B., Anderson, L.O., Malhi, Y., Saatchi, S., Gloor, E., 2014. Environmental change and the carbon balance of A mazonian forests. Biol. Rev. 89 (4), 913–931. https://doi.org/10.1111/brv.12088.

Arias, P.A., Fu, R., Vera, C., Rojas, M., 2015. A correlated shortening of the North and south American monsoon seasons in the past few decades. Clim. Dyn. 45 (11), 3183–3203. https://doi.org/10.1007/s00382-015-2533-1.

Barthem, R.B., Charvet-Almeida, P., Montag, L.F.A., Lanna, A.E., 2004. Global International Waters Assessment Amazon Basin, GIWA Regional Assessment 40 b. GIWA Regional Assessment Reports, p. 76.

Beck, H.E., Zimmermann, N.E., McVicar, T.R., Vergopolan, N., Berg, A., Wood, E.F., 2018. Present and future Köppen-Geiger climate classification maps at 1-km resolution. Sci. Data 5 (1), 1–12. https://doi.org/10.1038/sdata.2018.214.

Bedia, J., Baño-Medina, J., Legasa, M.N., Iturbide, M., Manzanas, R., Herrera, S., Gutiérrez, J.M., 2020. Statistical downscaling with the downscaleR package (v3.1.0): contribution to the VALUE intercomparison experiment. Geosci. Model Dev. 13 (3), 1711–1735. https://doi.org/10.5194/gmd-13-1711-2020.

Boucher, M.-A., Tremblay, D., Delorme, L., Perreault, L., Anctil, F., 2012. Hydro-economic assessment of hydrological forecasting systems. J. Hydrol. 416, 133–144. https://doi.org/10.1016/j.jhydrol.2011.11.042.

Brown, J.D., Demargne, J., Seo, D.J., Liu, Y., 2010. The Ensemble Verification System (EVS): A software tool for verifying ensemble forecasts of hydrometeorological and hydrologic variables at discrete locations. Environ. Model. Softw. 25 (7), 854–872. https://doi.org/10.1016/j.envsoft.2010.01.009.

Bustamante, J.F., Gomes, J.L., Chou, S.C., 2006, April. 5-year Eta model seasonal forecast climatology over South America. In: International Conference on Southern Hemisphere Meteorology and Oceanography, 8, pp. 24–28.

Bustamante, J.F., Chou, S.C., Sueiro, G., 2012. 10-year Eta model seasonal forecast climatology over South America. In: European Geoscience Union, General Assembly 2012. 22–27, April 2012, Vienna, Austria.

Cavalcanti, I.F., Marengo, J.A., Satyamurty, P., Nobre, C.A., Trosnikov, I., Bonatti, J.P., Camargo, H., 2002. Global climatological features in a simulation using the CPTEC–COLA AGCM. J. Clim. 15 (21), 2965–2988. https://doi.org/10.1175/1520-0442(2002)015<2965:GCFIAS>2.0.CO;2.

Chen, F., Janjić, Z., Mitchell, K., 1997. Impact of atmospheric surface-layer parameterizations in the new land-surface scheme of the NCEP mesoscale Eta model. Bound.-Layer Meteorol. 85 (3), 391–421. https://doi.org/10.1023/A:1000531001463.

Chou, S.C., Bustamante, J.F., Gomes, J.L., 2005. Evaluation of Eta Model seasonal precipitation forecasts over South America. Nonlinear Process. Geophys. 12 (4), 537–555. https://doi.org/10.5194/npg-12-537-2005.

Chou, S.C., Marengo, J.A., Lyra, A.A., Sueiro, G., Pesquero, J.F., Alves, L.M., Kay, G., Betts, R., Chagas, D.J., Gomes, J.L., 2012. Downscaling of South America present climate driven by 4-member HadCM3 runs. Clim. Dyn. 38, 635–653. https://doi.org/10.1007/s00382-011-1002-8.

Chou, S.C., Dereczynski, C., Gomes, J.L., Pesquero, J.F., Avila, A., Resende, N.C., Bustamante, J.F.F., 2020. Ten-year seasonal climate reforecasts over South America using the Eta regional climate model. An. Acad. Bras. Cienc. 92 https://doi.org/10.1590/0001-3765202020181242.

Cloke, H.L., Pappenberger, F., 2009. Ensemble flood forecasting: a review. J. Hydrol. 375 (3), 613–626. https://doi.org/10.1016/j.jhydrol.2009.06.005.

Collischonn, W., Haas, R., Andreolli, I., Tucci, C.E.M., 2005. Forecasting River Uruguay flow using rainfall forecasts from a regional weather-prediction model. J. Hydrol. 305 (1), 87–98. https://doi.org/10.1016/j.jhydrol.2004.08.028.

Collischonn, W., Morelli Tucci, C.E., Clarke, R.T., Chou, S.C., Guilhon, L.G., Cataldi, M., Allasia, D., 2007. Medium-range reservoir inflow predictions based on quantitative precipitation forecasts. J. Hydrol. 344 (1), 112–122. https://doi.org/10.1016/j.jhydrol.2007.06.025.

Crochemore, L., Ramos, M.H., Pappenberger, F., 2016. Bias correcting precipitation forecasts to improve the skill of seasonal streamflow forecasts. Hydrol. Earth Syst. Sci. 20 (9), 3601–3618. https://doi.org/10.5194/hess-20-3601-2016.

Demargne, J., Brown, J., Liu, Y., Seo, D.J., Wu, L., Toth, Z., Zhu, Y., 2010. Diagnostic verification of hydrometeorological and hydrologic ensembles. Atmos. Sci. Lett. 11 (2), 114–122. https://doi.org/10.1002/asl.261.

Doswell III, C.A., Davies-Jones, R., Keller, D.L., 1990. On summary measures of skill in rare event forecasting based on contingency tables. Weather Forecast. 5 (4), 576–585. https://doi.org/10.1175/1520-0434(1990)005<0576:OSMOSI>2.0.CO;2.

Espinoza, J.C., Marengo, J.A., Ronchail, J., Carpio, J.M., Flores, L.N., Guyot, J.L., 2014. The extreme 2014 flood in South-Western Amazon basin: the role of tropical-subtropical South Atlantic SST gradient. Environ. Res. Lett. 9 (12), 124007 https://doi.org/10.1088/1748-9326/9/12/124007.

Fan, Y., Miguez-Macho, G., 2010. Potential groundwater contribution to Amazon evapotranspiration. Hydrol. Earth Syst. Sci. 14 (10), 2039. https://doi.org/10.5194/hess-14-2039-2010.

Fan, F.M., Collischonn, W., Meller, A., Botelho, L.C.M., 2014. Ensemble streamflow forecasting experiments in a tropical basin: the São Francisco river case study. J. Hydrol. 519, 2906–2919. https://doi.org/10.1016/j.jhydrol.2014.04.038.

Fels, S.B., Schwarzkopf, M.D., 1975. The simplified exchange approximation: a new method for radiative transfer calculations. J. Atmos. Sci. 32, 1475–1488. https://doi.org/10.1175/1520-0469(1975)032<1475:TSEAAN>2.0.CO;2.

Ferrier, B.S., Jin, Y., Lin, Y., Black, T., Rogers, E., DiMego, G., 2002, August. Implementation of a new grid-scale cloud and precipitation scheme in the NCEP Eta model. In: Conference on weather analysis and forecasting, 19. AMS, pp. 280–283.

Gloor, M.R.J.W., Brienen, R.J., Galbraith, D., Feldpausch, T.R., Schöngart, J., Guyot, J.L., Phillips, O.L., 2013. Intensification of the Amazon hydrological cycle over the last two decades. Geophys. Res. Lett. 40 (9), 1729–1733. https://doi.org/10.1002/grl.50377.

Guimberteau, M., Ronchail, J., Espinoza, J.C., Lengaigne, M., Sultan, B., Polcher, J., Ciais, P., 2013. Future changes in precipitation and impacts on extreme streamflow over Amazonian sub-basins. Environ. Res. Lett. 8 (1), 014035 https://doi.org/10.1088/1748-9326/8/1/014035.

Guyot, J.L., Fillzola, N., Quintanilla, J., Cortez, J., 1996. Dissolved solids and suspended sediment yields in the Rio Madeira basin, from the Bolivian Andes to the Amazon. IAHS Publ. 55–64.

Hamilton, S.K., Sippel, S.J., Melack, J.M., 2002. Comparison of inundation patterns among major South American floodplains. J. Geophys. Res.-Atmos. 107 (D20), LBA–5. https://doi.org/10.1029/2000JD000306.

Iturbide, M., Bedia, J., Herrera, S., Baño-Medina, J., Fernández, J., Frías, M.D., Gutiérrez, J.M., 2019. The R-based climate4R open framework for reproducible climate data access and post-processing. Environ. Model. Softw. 111, 42–54. https://doi.org/10.1016/j.envsoft.2018.09.009.

Janjic, Z., 1979. Forward-backward scheme modified to prevent two-grid-interval noise and its application in sigma coordinate models. Contrib. Atmos. Phys 52, 69–84.

Janjić, Z.I., 1984. Nonlinear advection schemes and energy cascade on semi-staggered grids. Mon. Weather Rev. 112 (6), 1234–1245.

Janjić, Z.I., 1994. The step-mountain eta coordinate model: further developments of the convection, viscous sublayer, and turbulence closure schemes. Mon. Weather Rev. 122, 927–945. https://doi.org/10.1175/1520-0493(1994)122<0927:TSMECM>2.0.CO;2.

Kain, J.S., 2004. The Kain–Fritsch convective parameterization: an update. J. Appl. Meteorol. 43 (1), 170–181. https://doi.org/10.1175/1520-0450(2004)043<0170:TKCPAU>2.0.CO;2.

Kolachian, R., Saghafian, B., 2019. Deterministic and probabilistic evaluation of raw and post processed sub-seasonal to seasonal precipitation forecasts in different precipitation regimes. Theor. Appl. Climatol. 137 (1), 1479–1493. https://doi.org/10.1007/s00704-018-2680-5.

Lacis, A.A., Hansen, J., 1974. A parameterization for the absorption of solar radiation in the earth's atmosphere. J. Atmos. Sci. 31, 118–133. https://doi.org/10.1175/1520-0469(1974)031<0118:APFTAO>2.0.CO;2.

Latrubesse, E.M., Arima, E.Y., Dunne, T., Park, E., Baker, V.R., d'Horta, F.M., Baker, P.A., 2017. Damming the rivers of the Amazon basin. Nature 546 (7658), 363–369. https://doi.org/10.1038/nature22333.

Lenderink, G., Buishand, A., Deursen, W.V., 2007. Estimates of future discharges of the river Rhine using two scenario methodologies: direct versus delta approach. Hydrol. Earth Syst. Sci. 11 (3), 1145–1159. https://doi.org/10.5194/hess-11-1145-2007.

Li, H., Sheffield, J., Wood, E.F., 2010. Bias correction of monthly precipitation and temperature fields from Intergovernmental Panel on climate Change AR4 models using equidistant quantile matching. J. Geophys. Res.-Atmos. 115 (D10) https://doi.org/10.1029/2009JD012882.

Liu, X., Wu, T., Yang, S., Li, T., Jie, W., Zhang, L., Nie, S., 2017. MJO prediction using the sub-seasonal to seasonal forecast model of Beijing climate Center. Clim. Dyn. 48 (9–10), 3283–3307. https://doi.org/10.1007/s00382-016-3264-7.

Lorenz, E.N., 1963. Deterministic nonperiodic flow. J. Atmos. Sci. 20 (2), 130–141. https://doi.org/10.1175/1520-0469(1963)020<0130:DNF>2.0.CO;2.

Marengo, J.A., Soares, W.R., Saulo, C., Nicolini, M., 2004. Climatology of the low-level jet east of the Andes as derived from the NCEP–NCAR reanalyses: Characteristics and temporal variability. J. Clim. 17 (12), 2261–2280. https://doi.org/10.1175/1520-0442(2004)017<2261:COTLJE>2.0.CO;2.

Marengo, J., Nobre, C.A., Betts, R.A., Cox, P.M., Sampaio, G., Salazar, L., 2009. Global warming and climate change in Amazonia: climate-vegetation feedback and impacts on water resources. Amazon. Glob. Change 186, 273–292. https://doi.org/10.1029/2008GM000744.

Marengo, J.A., Tomasella, J., Alves, L.M., Soares, W.R., Rodriguez, D.A., 2011. The drought of 2010 in the context of historical droughts in the Amazon region. Geophys. Res. Lett. 38 (12) https://doi.org/10.1029/2011GL047436.

Martens, B., Miralles, D.G., Lievens, H., Van Der Schalie, R., De Jeu, R.A., Fernández-Prieto, D., Verhoest, N.E., 2017. GLEAM v3: Satellite-based land evaporation and root-zone soil moisture. Geosci. Model Dev. 10 (5), 1903–1925. https://doi.org/10.5194/gmd-10-1903-2017.

Meller, A., 2012. Short Term Ensemble Flood Forecasting (Previsão de Cheias por Conjunto em Curto Prazo). PhD Thesis. Federal University of Rio Grande do Sul. Hydraulic Research Institute, p. 224. http://hdl.handle.net/10183/70057.

Meller, A., Collischonn, W., Fan, F.M., Buarque, D.C., Paiva, R.C.D., Dias, P., Moreira, D., 2014. Short term ensemble flood forecasting. Rev. Bras. Recur. Hidr. 19, 33–49. https://doi.org/10.1590/2318-0331.011616004.

Mellor, G.L., Yamada, T., 1982. Development of a turbulence closure model for geophysical fluid problems. Rev. Geophys. 20, 851–875. https://doi.org/10.1029/RG020i004p00851.

Mesinger, F., 1984. A blocking technique for representation of mountains in atmospheric models. Riv. Meteorol. Aeronaut. 44, 195–202. http://pascal-francis.inist.fr/vibad/index.php?action=getRecordDetail&idt=8419610.

Mesinger, F., Chou, S.C., Gomes, J.L., Jovic, D., Bastos, P., Bustamante, J.F., Veljovic, K., 2012. An upgraded version of the Eta model. Meteorog. Atmos. Phys. 116 (3), 63–79. https://doi.org/10.1007/s00703-012-0182-z.

Miralles, D.G., Holmes, T.R.H., De Jeu, R.A.M., Gash, J.H., Meesters, A.G.C.A., Dolman, A.J., 2011. Global land-surface evaporation estimated from satellite-based observations. Hydrol. Earth Syst. Sci. 15 (2), 453–469. https://doi.org/10.5194/hess-15-453-2011.

Molina-Carpio, J., Espinoza, J.C., Vauchel, P., Ronchail, J., Gutierrez Caloir, B., Guyot, J. L., Noriega, L., 2017. Hydroclimatology of the Upper Madeira River basin: spatio-temporal variability and trends. Hydrol. Sci. J. 62 (6), 911–927. https://doi.org/10.1080/02626667.2016.1267861.

Molinier, M., Guyot, J.L., De Oliveira, E., Guimarães, V., Chaves, A., 1995. Hydrologie du bassin de l'Amazone. Proc. Grands Bassins Fluviaux Péri-atlantiques 1, 335–344.

Monin, A.S., Obukhov, A.M., 1954. Basic laws of turbulent mixing in the surface layer of the atmosphere. Contrib. Geophys. Inst. Acad. Sci. USSR 151 (163), e187.

Moran-Zuloaga, D., Ditas, F., Walter, D., Saturno, J., Brito, J., Carbone, S., Godoi, R.H., 2018. Long-term study on coarse mode aerosols in the Amazon rain forest with the frequent intrusion of Saharan dust plumes. Atmos. Chem. Phys. 18 (3), 10055–10088. https://doi.org/10.5194/acp-18-10055-2018.

Navarro, G., Maldonado, M., 2002. Geografía ecológica de Bolivia: Vegetación y ambientes acuáticos. Centro de Ecología Simón I. Patiño, Departamento de Difusión, Cochabamba, Bolivia, p. 719.

Nobre, C.A., Obregón, G.O., Marengo, J.A., Fu, R., Poveda, G., 2009. Characteristics of Amazonian climate: main features. Amazon. Glob. Change 186, 149–162.

Ovando, A., Tomasella, J., Rodriguez, D.A., Martinez, J.M., Siqueira-Junior, J.L., Pinto, G.L.N., Von Randow, C., 2016. Extreme flood events in the Bolivian Amazon wetlands. J. Hydrol. Region. Stud. 5, 293–308. https://doi.org/10.1016/j.ejrh.2015.11.004.

Parrens, M., Al Bitar, A., Frappart, F., Paiva, R., Wongchuig, S., Papa, F., Kerr, Y., 2019. High resolution mapping of inundation area in the Amazon basin from a combination of L-band passive microwave, optical and radar datasets. Int. J. Appl. Earth Obs. Geoinf. 81, 58–71. https://doi.org/10.1016/j.jag.2019.04.011.

Paulson, C.A., 1970. The mathematical representation of wind speed and temperature profiles in the unstable atmospheric surface layer. J. Appl. Meteorol. Climatol. 9 (6), 857–861. https://doi.org/10.1175/1520-0450(1970)009<0857:TMROWS>2.0.CO;2.

Piani, C., Haerter, J., Coppola, E., 2010. Statistical bias correction for daily precipitation in regional climate models over Europe. Theor. Appl. Climatol. 99 (1–2), 187–192. https://doi.org/10.1007/s00704-009-0134-9.

Pilotto, I.L., Chou, S.C., Nobre, P., 2012. Seasonal climate hindcasts with Eta model nested in CPTEC coupled ocean–atmosphere general circulation model. Theor. Appl. Climatol. 110 (3), 437–456. https://doi.org/10.1007/s00704-012-0633-y.

Rozante, J.R., Moreira, D.S., de Goncalves, L.G.G., Vila, D.A., 2010. Combining TRMM and surface observations of precipitation: technique and validation over South America. Weather Forecast. 25 (3), 885–894. https://doi.org/10.1175/2010WAF2222325.1.

Rozante, J.R., Gutierrez, E.R., Fernandes, A.D.A., Vila, D.A., 2020. Performance of precipitation products obtained from combinations of satellite and surface observations. Int. J. Remote Sens. 41 (19), 7585–7604. https://doi.org/10.1080/01431161.2020.1763504.

Schwanenberg, D., Fan, F.M., Naumann, S., Kuwajima, J.I., Montero, R.A., Dos Reis, A. A., 2015. Short-term reservoir optimization for flood mitigation under meteorological and hydrological forecast uncertainty. Water Resour. Manag. 29 (5), 1635–1651. https://doi.org/10.1007/s11269-014-0899-1.

Sestini, M.F., Alvalá, R.D.S., Mello, E.M.K., Valeriano, D.D.M., Chan, C.S., Nobre, C.A., Paiva, J.D.C., Reimer, E.D.S., 2002. Elaboração de Mapas de Vegetação para Utilização em Modelos Meteorológicos e Hidrológicos. São José dos Campos: INPE-8972-RPQ/730.

Shrestha, P., Sulis, M., Simmer, C., Kollet, S., 2015. Impacts of grid resolution on surface energy fluxes simulated with an integrated surface-groundwater flow model. *Hydrol. Earth Syst.* Sci. 19, 4317–4326. https://doi.org/10.5194/hess-19-4317-2015.

Shrestha, S., Chapagain, R., Babel, M.S., 2017. Quantifying the impact of climate change on crop yield and water footprint of rice in the Nam Oon Irrigation Project, Thailand. Sci. Total Environ. 599, 689–699. https://doi.org/10.1016/j.scitotenv.2017.05.028.

Siddique, R., Mejia, A., 2017. Ensemble streamflow forecasting across the US Mid-Atlantic region with a distributed hydrological model forced by GEFS reforecasts. J. Hydrometeorol. 18 (7), 1905–1928. https://doi.org/10.1175/JHM-D-16-0243.1.

Silva, B.C., Tucci, C.E.M., Collischonn, W., 2006. Previsão de vazão com modelos hidroclimáticos. Rev. Bras. Recur. Hidr. 11 (3), 15–30. https://doi.org/10.21168/rbrh.v11n3.p15-29.

Silva, B.C., Collischonn, W., Tucci, C.E.M., Clarke, R.T., Corbo, M.D., 2007. Previsão hidroclimática de vazão de curto prazo na bacia do rio São Francisco. Rev. Bras. Recur. Hidr. 12, 31–47. https://doi.org/10.21168/rbrh.v12n3.p31-41.

Tanessong, R.S., Vondou, D.A., Igri, P.M., Kamga, F.M., 2012. Evaluation of Eta weather forecast model over Central Africa. Atmosph. Clim. Sci. 2 (4), 532–537.

Teng, J., Potter, N.J., Chiew, F.H.S., Zhang, L., Wang, B., Vaze, J., Evans, J.P., 2015. How does bias correction of regional climate model precipitation affect modelled runoff? Hydrol. Earth Syst. Sci. 19, 711–728. https://doi.org/10.5194/hess-19-711-2015.

Themeßl, M.J., Gobiet, A., Heinrich, G., 2012. Empirical-statistical downscaling and error correction of regional climate models and its impact on the climate change signal. Clim. Chang. 112 (2), 449–468. https://doi.org/10.1007/s10584-011-0224-4.

Tian, D., Wood, E.F., Yuan, X., 2017. CFSv2-based sub-seasonal precipitation and temperature forecast skill over the contiguous United States. Hydrol. Earth Syst. Sci. 21 (3), 1477–1490. https://doi.org/10.5194/hess-21-1477-2017.

Tucci, C.E.M., Clarke, R.T., Collischonn, W., da Silva Dias, P.L., de Oliveira, G.S., 2003. Long-term flow forecasts based on climate and hydrologic modeling: Uruguay River basin. Water Resour. Res. 39 (7) https://doi.org/10.1029/2003WR002074.

Van der Ent, R.J., Savenije, H.H., Schaefli, B., Steele-Dunne, S.C., 2010. Origin and fate of atmospheric moisture over continents. Water Resour. Res. 46 (9) https://doi.org/10.1029/2010WR009127.

Verkade, J.S., Brown, J.D., Reggiani, P., Weerts, A.H., 2013. Post-processing ECMWF precipitation and temperature ensemble reforecasts for operational hydrologic forecasting at various spatial scales. J. Hydrol. 501, 73–91. https://doi.org/10.1016/j.jhydrol.2013.07.039.

Walker, D.P., Birch, C.E., Marsham, J.H., Scaife, A.A., Graham, R.J., Segele, Z.T., 2019. Skill of dynamical and GHACOF consensus seasonal forecasts of East African rainfall. Clim. Dyn. 53 (7), 4911–4935. https://doi.org/10.1007/s00382-019-04835-9.

Wanzeler da Costa, C.P., Satyamurty, P., 2016. Inter-hemispheric and inter-zonal moisture transports and monsoon regimes. Int. J. Climatol. 36 (15), 4705–4722. https://doi.org/10.1002/joc.4662.

Weng, W., Luedeke, M.K., Zemp, D.C., Lakes, T., 2018. Aerial and surface rivers: downwind impacts on water availability from land use changes in Amazonia. Hydrol. Earth Syst. Sci. 22, 911–927. https://doi.org/10.5194/hess-22-911-2018.

White, C.J., Carlsen, H., Robertson, A.W., Klein, R.J., Lazo, J.K., Kumar, A., Zebiak, S.E., 2017. Potential applications of subseasonal-to-seasonal (S2S) predictions. Meteorol. Appl. 24 (3), 315–325. https://doi.org/10.1002/met.1654.

Wilks, D.S., 2011. Statistical Methods in the Atmospheric Sciences, vol. 100. Academic Press. https://doi.org/10.1016/B978-0-12-385022-5.00008-7.

Yuan, X., Wood, E.F., Ma, Z., 2015. A review on climate-model-based seasonal hydrologic forecasting: physical understanding and system development. Wiley Interdiscip. Rev. Water 2 (5), 523–536. https://doi.org/10.1002/wat2.1088.

Zanin, P.R., Satyamurty, P., 2021. Interseasonal and Interbasins Hydrological Coupling in South America. J. Hydrometeorol. 22 (6), 1609–1625. https://doi.org/10.1175/JHM-D-20-0080.1.

Zemp, D.C., Schleussner, C.F., Barbosa, H.M., Hirota, M., Montade, V., Sampaio, G., Rammig, A., 2017. Self-amplified Amazon forest loss due to vegetation-atmosphere feedbacks. Nat. Commun. 8 (1), 1–10. https://doi.org/10.1038/ncomms14681.

Zhao, Q., Black, T.L., Baldwin, M.E., 1997. Implementation of the cloud prediction scheme in the Eta Model at NCEP. Weather Forecast. 12, 697–712. https://doi.org/10.1175/1520-0434(1997)012<0697:IOTCPS>2.0.CO;2.

Zhao, T., Bennett, J.C., Wang, Q.J., Schepen, A., Wood, A.W., Robertson, D.E., Ramos, M. H., 2017. How suitable is quantile mapping for postprocessing GCM precipitation forecasts? J. Clim. 30 (9), 3185–3196. https://doi.org/10.1175/JCLI-D-16-0652.1.